Comparative Performance Evaluation of Conventional and Folded Detector Structures for X-ray imaging

By

Robin Ray

A Thesis

in

The Department

of

Electrical and Computer Engineering

Presented in Partial Fulfillment of the Requirements for the Degree of Master of Applied Science (M.A.Sc) at

Concordia University

Montreal, Quebec, Canada

August, 2023

CONCORDIA UNIVERSITY
SCHOOL OF GRADUATE STUDIES

This is to certify that the thesis prepared

By: Robin Ray

Entitled: "Comparative Performance Evaluation of Conventional and Folded Detector Structures for X-ray imaging "

and submitted in partial fulfillment of the requirements for the degree of

Master of Applied Science

Complies with the regulations of this University and meets the accepted standards with respect to originality and quality.

Signed by the final examining committee:

_____ Chair
Dr. Hassan Rivaz

_____ Examiner, External
Dr. Anjan Bhowmick

_____ Examiner
Dr. Hassan Rivaz

_____ Supervisor
Dr. M. Z. Kabir

Approved by: _____
Dr. Yousef Shayan, Chair
Department of Electrical and Computer Engineering

_____20_____ _____
Dr. Mourad Debbabi, Dean
Faculty of Engineering and Computer Science

ABSTRACT

Comparative Performance Evaluation of Conventional and Folded Detector Structures for X-ray imaging

Robin Ray

X-ray photoconductor-based flat-panel X-ray imagers (FPXIs) produce superior X-ray image as compared to scintillator-based detectors and are the commercially available digital X-ray detectors for mammography. These detectors are, at present, under scrutiny for use in general radiography, fluoroscopy, tomosynthesis and portal imaging. Although amorphous selenium (*a*-Se) is the most successful photoconductor, recently, Hybrid Organic−Inorganic Perovskites (HOIPs) receive much attention for this application because of their good charge transport properties, higher attenuation coefficient and solution-based cheaper process techniques. These detectors need high detective quantum efficiency (DQE) for getting clear X-ray image.

The photoconductor layer thickness plays a very important role in conventional detector structure (i.e., a photoconductor layer is sandwiched between two electrodes where charges are collected in corresponding pixels) on imaging performances. A relatively thicker layer is required for better sensitivity. However, the thicker layer contributes to more noise and signal spreading as carriers must travel a longer distance to reach the electrodes, and thus adversely affects image resolution and DQE). In a folded structure, charge carriers travel perpendicular to the direction of incident X-rays and thus the X-ray quantum efficiency can be improved using a thicker layer without affecting the charge collection by keeping the charge collecting electrodes at a reasonable distance. It is essential to do a comparative analysis on DQE performance of both conventional and folded structure.

This dissertation focuses on developing mathematical model for studying the DQE of both folded and conventional detector structures by incorporating the quantum noise due to random charge carrier trapping in the cascaded linear system model. An analytical expression for the

variance of charge collection in folded structure has been developed. The optimum values of photoconductor layer thickness and spacing between electrodes for maximizing the DQE under various material parameters and detector operating conditions are also investigated. The DQE critically depends on the detector thickness. As a result, the optimum DQE can be even below 0.3 for certain values of material and device parameters in conventional structure. On the contrary, the folded structure provides more design flexibility for achieving high DQE (even higher than 0.7) by adjusting the distance between electrodes without compromising the quantum efficiency. Since the folded structure is more complex than the conventional structure, one should prefer the folded structure if the photoconductor possesses relatively low linear attenuation coefficient for higher energy X-rays together with poor charge carrier transport properties. Moreover, it has also been found that the poly $MAPbI_3$ detector shows significantly better DQE performance than the Amorphous Selenium Detector.

To all the people
who were kind to me.

Acknowledgements

A thesis work in master's level requires ample amount of hard work as well as proper guidance. The guidance of a good supervisor can work as the biggest motivation to conduct quality research. I am grateful to my supervisor M. Zahangir Kabir for accepting me as a student in his group. His funding and guidance ensured a stable environment for me to put my attention in research.

During my research, I figured out there are numerous theoretical concepts I should know to conduct the research. He took a course based on "Radiation Detectors for Medical Imaging", which has helped me a lot to understand the insights of the work. During my research work, many times I have gone through different challenges. He has always given me proper suggestions so that I can deal with the complexity of the work.

The attitude toward a student can greatly impact the performance of a student. If a student feels free with his/her supervisor, it gets easier to be comfortable with his/her work. M. Zahangir Kabir has a personality mixed of both responsibility and kindness, which has given me enough confidence to conduct a discussion with him with no hesitation, which made me more interested in my research task.

He spent many hours helping me to analyze data, curves, planning research direction and proofreading of my thesis as well as provide suggestions. I will be grateful to him for all these reasons.

Table of Contents

List of Tables

List of Figures

LIST OF SYMBOLS

α	Linear attenuation coefficient
δ	absorption depth
η	Photogeneration efficiency
Φ_0	Photon fluence
μ	Carrier mobility
τ	Carrier lifetime
μ_h	Hole mobility
μ_e	Electron mobility
τ_h	Hole lifetime
τ_e	Electron lifetime
e	Electronic charge
F	Applied electric field
d	Distance between electrodes, thickness of conventional device structure
l	Thickness of folded device structure
X	X-ray exposure
E	Energy of incident X-ray photon
η_{cc}	Charge collection efficiency

x	Distance along the photoconductor in x axis
y	Distance along photoconductor in y axis
E_{ab}	Average absorbed energy per X-ray photon
σ	Standard deviation
σ^2	Variance
N_e	Electronic noise
d_{foil}	Width of electrode
x_t	Schubweg of carrier which goes to top electrode
x_b	Schubweg of carrier which goes to bottom electrode
$W_{\pm}$	Electron hole pair creation energy

LIST OF ACRONYMS

AMFPI	Active-matrix flat panel imaging
AMA	Active-Matrix Array
EHP	Electron Hole Pair
DQE	Detective Quantum Efficiency
a-Se	Amorphous selenium
keV	Kilo Electron Volt
SNR	Signal to Noise Ratio
HOIP	Hybrid Organic-Inorganic Perovskites
poly-$MAPbI_3$	Polycrystalline Methylammonium Lead Iodide
MTF	Modulation Transfer Function
NPS	Noise Power Spectrum
TFT	Thin Film Transistor
KTC	Thermal noi

Chapter 1: Introduction

1.1 Background

X-ray was discovered by Wilhelm Conrad Roentgen (1845-1923) [1]. While he was working with cathode ray tube in his laboratory, he discovered a fluorescent glow which he named X-ray. It is considered as a revolutionary discovery which has brought impressive development in a wide range of applications including diagnostics [2][3][4], non-destructive testing (NDT) [5][6][7][8][9] and scientific research [10]. For disease detection, staging and treatment, X-ray provided us with a variety of tools and techniques.

Flat panel detector played a big role in the development of X-ray imaging technology [11], especially direct flat panel digital X-ray detectors. It played an important role for the transition from analog to digital X-ray imaging.

In figure 1.1, the simplified operating principle of a flat panel X-ray detector is illustrated. Here, the X-ray photons are passing through the hand (object), and behind the object there is a sensor, which is connected to an analyzing device. X-ray image incidents on the sensor, and the sensor converts the image to a digital image. This digital image is sent to the computer for further procedure.

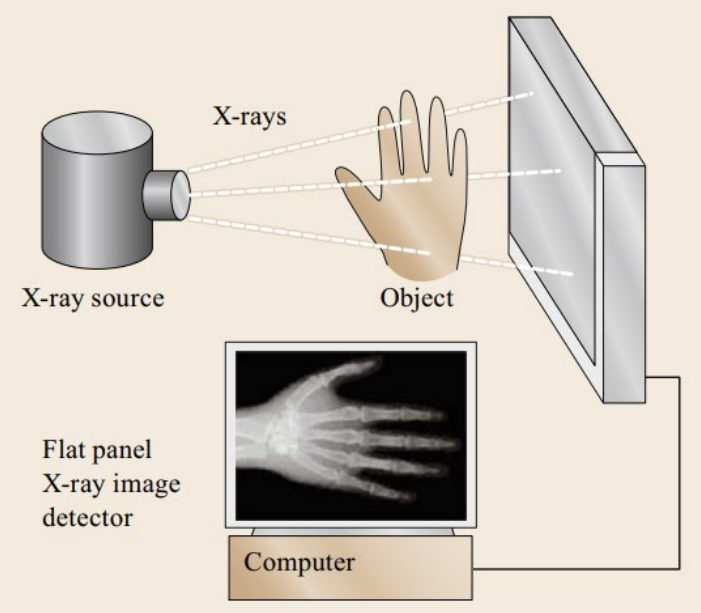

Figure 1.1: Active-matrix flat panel imaging (AMFPI) system [15]

Large area integrated circuit or active-matrix array (AMA) is the most practical flat panel digital detector, which is used for mammography, fluoroscopy, chest radiology, and many other applications. Flat panel detectors that include active-matrix array are known as active matrix flat-panel imagers (AMFPI). Different materials can be used to develop this structure. A practical schematic diagram of AMEPI is shown in figure 1.2.

The active-matrix array addresses the pixels. Each of the pixels collect charge, and the collected charge is proportional to the X-ray radiation incident on it. For indirect photodetector, at first the X-ray is converted to visible light, then the visible light is converted to charge. For direct photodetector, X-ray is directly converted to charge instead of converting into visible light. The charges stored in the pixels are read out by scanning the arrays row by row and multiplexing parallel columns of the array. Signal is received by a computer for display and storage. [12]

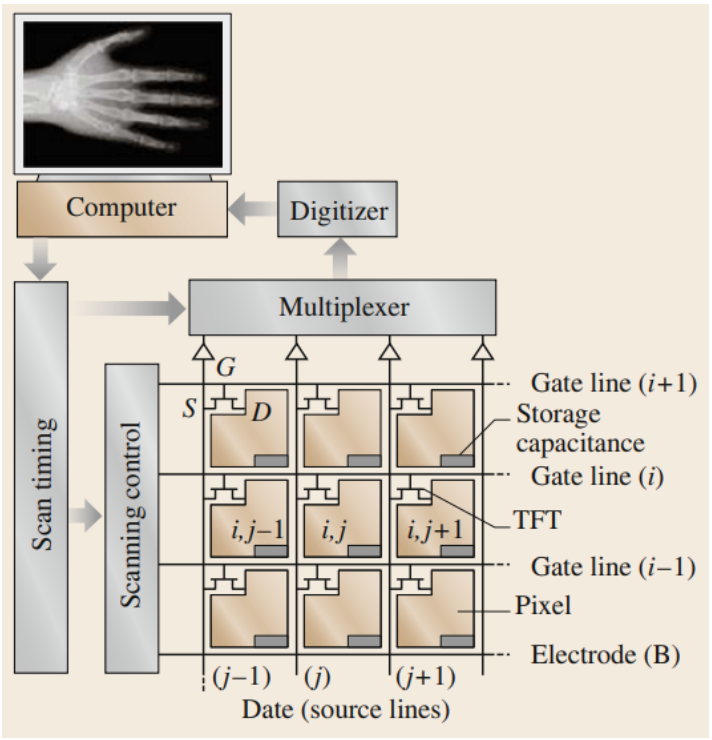

Figure 1.2: Schematic diagram of an active-matrix array (AMFPI). Charge is distributed in panel's pixels, and these are read out using multiplexors and scanning control system. [2]

It is necessary to figure out a suitable material for constructing an X-ray photodetector. There are many materials which can be used for developing photodetector such as amorphous selenium, poly-$MAPbI_3$, poly-CdZnTe, GaAs, HgI_2, PbI_2 etc.

Ideal photoconductor materials should have the following properties [2]:

1. Incident X-ray photons/radiation needs to be absorbed within the photoconductor thickness. The absorption depth (δ) of X-ray should be less than the photoconductor thickness so that most of the incident X-rays are absorbed within the photoconductor layer.
2. Materials with high X-ray sensitivity should be used to build photoconductor. The material should be able to produce a large number of electron hole pairs (EHP) for per unit radiation. This means that energy required to create a single EHP (i.e., the ionization energy, W_i) should be low.

3. There should be less deep trapping for electrons and holes. The schubweg $\mu\tau F$ should be more than photoconductor thickness. Here μ is carrier drift mobility, τ is carrier lifetime and F is electric field. The average length a carrier (electron/hole) travels before it gets trapped is called schubweg.
4. The diffusion of electrons and holes should be less than their drift.
5. Dark current acts as a source of noise in photoconductor, so dark current should be low.
6. The photoconductor properties should be consistent with time, means properties should not change with time.
7. The material should be conveniently and uniformly deposited over a large area.

Due to low dark current, good charge-transport properties, and convenient low-temperature deposition over a large area, amorphous selenium (a-Se) has been used for a long time for direct conversion detectors [13]. But when we compare with HgI_2 or CdZnTe, the ionization energy, $W_{i,}$ is large for *a-Se*. As a result, it has relatively lower intrinsic X-ray sensitivity [14]. As well as most of the polycrystalline detectors exhibit large dark current under high fields or show incomplete charge collection [15][16]. At the same time, poly-$MAPbI_3$ requires less energy to create electron hole pair. Hence, it will provide better quantum efficiency and higher detective quantum efficiency (DQE) [17][18].

1.2 Research motivation

X-ray photoconductor based flat panel X-ray imagers (FPXIs) produce better quality image as compared to scintillator-based detectors and are commercially available for mammography [19][20]. Presently, these detectors are under test to use in other medical applications such as general radiography, fluoroscopy and tomosynthesis [21][22]. Amorphous selenium (*a*-Se) is a popular material to use in photoconductor-based X-ray detector because of the physical properties such as low dark current and good charge transport properties. It can also be deposited conveniently over large area at low temperature. But there is one serious drawback of *a*-Se, which is its lower intrinsic X-ray sensitivity. It happens due to its large ionization energy, $W_{i,}$ which is minimum radiation energy required to create an electron hole pair (EHP). For comparison, the value of W_i in *a*-Se is about 45 eV at the typical operating electric field of 10

V/μm where the value of W_i is 5–6 eV for other X-ray photoconductors such as polycrystalline HgI_2 or CdZnTe [23]. Lower ionization energy W_i causes more EHP generation and improves SNR and signal strength (i.e., higher X-ray sensitivity).

When we deal with polycrystalline detectors, the basic underlying problem is that they exhibit either an unacceptably large dark current or they possess significantly low charge collection efficiency [23][24]. Dark current means a current that flows in the detector in absence of radiation. The use of Hybrid Organic-Inorganic Perovskites (HOIPs) in large area X-ray detector was first observed by Yakunin et al. [25] in 2015 when he demonstrated a prototype X-ray detector using a thick layer (~100 μm) of polycrystalline methylammonium lead iodide (poly-$MAPbI_3$ where MA is CH_3NH_3) perovskite photoconductor. It showed high dark current initially. Then Kim et al.[26] proposed a multilayer structure to reduce dark current using poly-$MAPbI_3$. They found low dark current, good X-ray sensitivity, but poor resolution in terms of modulation transfer function (MTF).

In conventional detector structure, photoconductor layer thickness plays a very important role in imaging performance [23]. In conventional structure, a photoconductor layer is sandwiched between two electrodes, and charges are collected at the corresponding pixels. A thicker layer is required for better sensitivity, but thicker layer contributes to more noise and signal spreading, as carriers must travel a longer distance to reach the electrode. As a result, the image resolution and detective quantum efficiency (DQE) are affected [27][28].

Recently Mescher et al. [29] proposed a folded structure, where charge carrier travel perpendicular to the direction of incident X-ray. Charge carrier transport mechanism in folded structure is similar to coplanar detector structure [30]. In folded structure, quantum efficiency can be improved using a thicker layer without affecting the charge collection, because charge collecting electrodes can be kept at a reasonable distance. However, they have used an oversimplified model to analyze the DQE. They did not consider the quantum noise due to random charge carrier trapping, which is an important factor to model detective quantum efficiency (DQE). Therefore, a comprehensive model is essential for accurate performance analysis.

1.3 Research objectives and tasks

As mentioned earlier, *a*-Se has some physical limitations to achieve high DQE as well as sensitivity. So, in this work, I am going to use both *a*-Se and poly-$MAPbI_3$ to compare their imaging performance. At the same time, my thesis will aim to develop mathematical model for calculating DQE of both conventional and folded structures, and to compare their imaging performances.

In this thesis, I am going to analyze detective quantum efficiency (DQE) using a cascaded linear system model for both conventional and folded structure detector by incorporating quantum noise due to random charge carrier trapping. The analytical expression of variance of charge collection for folded structure will be developed here. The optimum values of photoconductor layer thickness and spacing between electrodes for maximizing the DQE will be investigated under various material parameters and detector operating conditions.

I will obtain DQE characteristics for both conventional and folded structure for fluoroscopy and mammography using *a*-Se and poly-$MAPbI_3$ to figure out the relatively better material and model applicable for these medical applications.

1.4 Organization of the thesis

The thesis is organized as follows.

Chapter 2 provides some background knowledge required to understand the work undertaken in this thesis. Firstly, the physical structure of conventional and folded structure is explained. Following that, detective quantum efficiency (DQE) and different types of noise associated with X-ray detectors are described briefly. A general description and importance of cascaded linear system model is discussed in chapter 2.

In chapter 3, detective quantum efficiency (DQE) model is developed. At first, stochastic amplification is discussed with proper equations. Then both conventional and folded device

structures are discussed using cascaded linear system model. Each of the stages (such as X-ray attenuation, conversion gain, charge collection efficiency, electronic noise) of the linear models are discussed with mathematical expressions. The expression of DQE for both structures are obtained in this chapter.

In chapter 4, the results from the DQE model are shown for both conventional and folded structure. Fluoroscopy and mammography applications are the main concern of this chapter. At first, poly-$MAPbI_3$ is used to conduct the study. The different values of carrier mobility and lifetime was used to observe DQE characteristics. A comparison of conventional and folded structure for both medical applications are shown in this chapter. Then amorphous selenium was used to conduct the same study. At the end of this chapter, a conclusion has been drawn between amorphous selenium and poly-$MAPbI_3$ based on imaging performance.

Chapter 5 concludes this thesis by summarizing the main contributions made in this thesis, and suggesting some future work that can be undertaken.

Chapter 2: BACKGROUND CONCEPTS

2.1 Introduction

In this chapter, some background knowledge is provided to understand the work undertaken in this thesis. Firstly, the physical structure of conventional and folded structure is explained. Following that, detective quantum efficiency (DQE) and different types of noise associated with X-ray detectors are described briefly. A general description and importance of cascaded linear system model is also discussed in this chapter.

2.2 Conventional and Folded Structure

In chapter 1, conventional structure and folded structure were introduced. In this chapter, both structures will be described briefly.

Conventional Structure: In conventional structure, semiconductor material is sandwiched between two large area parallel plate electrodes. A bias voltage is applied between two electrodes. As a result, electric field F was established between the electrodes. In figure 2.1, the thickness of the photoconductor is denoted by d. The upper electrode is negatively biased. The incoming photons incident on the electrode surface. The photons are absorbed by the material and through direct conversion, electron-hole pairs are created. Because of the existing electric field F between electrodes, electron and holes are drifted in opposite direction. These electrons are collected in lower electrode, and the holes are collected in upper electrode.

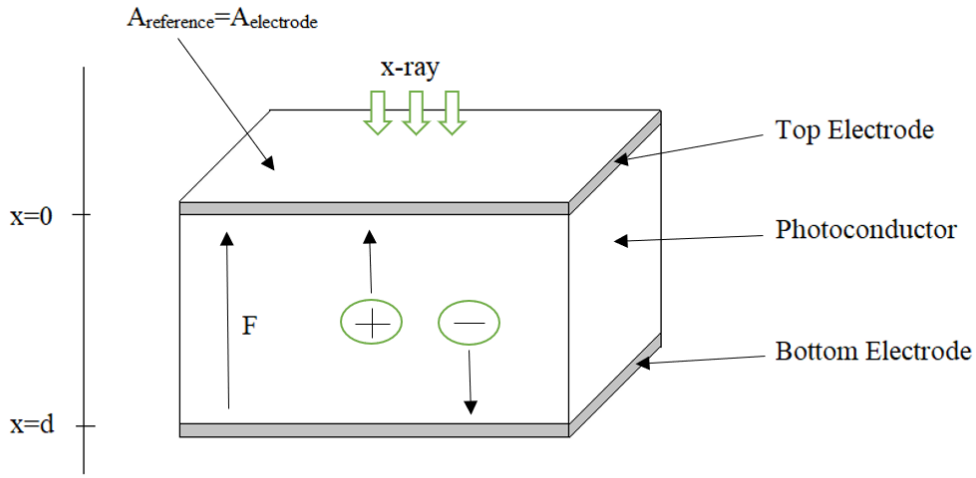

Figure 2.1. Conventional device structure for negatively biased top electrode. Upper and lower portion are parallel plate electrodes and middle portion is direct conversion material. Thickness of the photoconductor is denoted by *d*.

Folded Structure: In folded structure, photons are absorbed by the material parallel to the electrodes, where in conventional structure, photons are absorbed perpendicular to the electrodes. In fig 2.2, many pixels are placed together using folded design. In the middle pixel, X-ray photons are incident parallel to the electrodes in the semiconductor. The left electrode is negatively, and right electrode is positively biased. Because of the bias voltage, an electric field F is established between the electrodes. Through direct conversion, electron hole pairs are created in the material. The holes are drifted and collected in the left electrode, where the electrons are drifted and collected in right electrode.

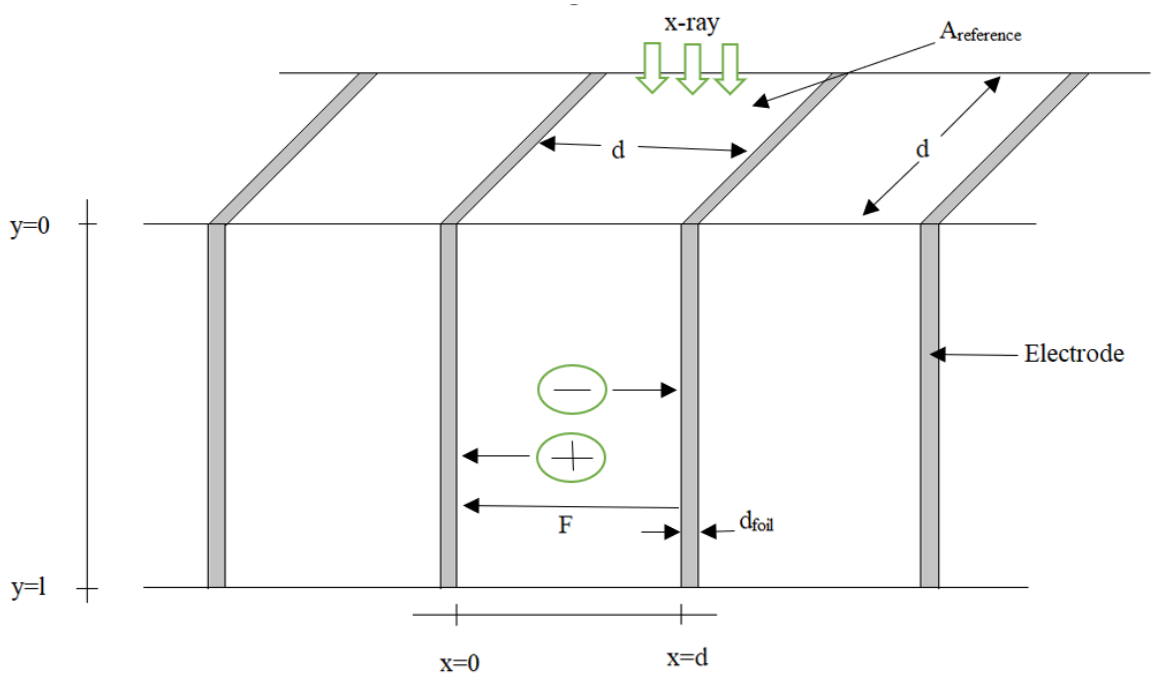

Figure 2.2. A folded device structure with three pixels. In every pixel, semiconductor material is sandwiched between two large area parallel plate electrodes. X-ray photons incident on the material parallel to the electrodes. Thickness and distance between electrodes are denoted by *l* and *d* respectively.

2.3: Detective Quantum Efficiency (DQE)

DQE is a measurement of effect of signal and noise performance. It measures the ability of a detector how good it is in transferring a signal relative to noise from input side to output side. Generally, it is expressed as a function of spatial frequency. In the case of medical radiology, it describes how effectively an X-ray imaging system can produce an image with a high signal-to-noise ratio (SNR) relative to an ideal detector.

During 1940, there had been huge interest about classifying the performance of signal and noise in different form of detectors, such as television and camera. Quantum efficiency was used to determine the performance of detector at that time, but there were other physical processes which were involved degrading quality of image. In 1946, Albert Rose proposed a concept about an equivalent quantum efficiency to describe performance of those detectors, which is now called as detective quantum efficiency. After some years, DQE was started using in medical imaging.

In the modern X-ray detector, due to various sources of statistical fluctuation, image quality degrades partially. If spatial frequency is *f*, then DQE(*f*) is described as [31]

$$DQE(f) = \frac{SNR_{out}^{\ 2}(f)}{SNR_{in}^{\ 2}(f)} \tag{2.1}$$

Where SNR_{in} and SNR_{out} are signal to noise ratio in input and output side of an image detector. For an idea detector, $DQE(f)$ is unity.

There are various forms of noise associated with an imaging system. They have been described below.

Quantum Noise: Quanta means number of particle or objects which can be counted, such as electron and photon. Because of random fluctuation of incident quanta, quantum noise is observed. It basically posses a theoretical limit of optical performance.

Electronic Noise: When quanta pass through detector element, they are read out by various electronic components. Each of those electronic components add an amount of electronic noise with the signal. This noise can have various forms such as thermal noise, dark noise, and amplifier noise. These noises play a significant role in degrading detector performance.

2.4: Cascaded Linear System Model

Cascaded linear system model is used to characterize the performance of imaging systems in terms of signal transfer and noise transfer relationship. In the cascaded linear model, an imaging system is described as a cascade of simple and independent elementary stages. In most cases, the input and output of each stage is a distribution of quanta. These quanta can be X-rays, light or electrons. The random nature of image quanta creates statistical fluctuations in image signal contributing to image formation. The signal and noise are passed through various stages such as gain, blurring, addition, aliasing in an imaging system. At each stage, the signal and NPS are calculated from the signal and NPS of previous stage and the characteristics of the current stage.

Cascaded linear system is useful because it helps to break down the imaging system into simple and independent terms, hence, the imaging properties can be determined separately. The complexity of understanding the detector performance reduces significantly.

There are three elementary processes that have important role in understanding signal and noise transfer. (a) stochastic amplification (b) stochastic blurring (c) deterministic blurring.

Stochastic amplification: For the stochastic gain stage *i,* the output mean signal quanta per unit area and noise power spectrum (NPS) arising from incident X-ray photon interactions at depth *x* from the radiation-receiving electrode are described using following equations [32][33],

$$\begin{aligned} \overline{\phi_i}(E,x) &= \overline{g_i}(E,x).\overline{\phi_{i-1}}(E,x) \\ S_{N_i}(E,x) &= \overline{g_i}^2(E,x).S_{N_{i-1}}(E,x) + \sigma_{g_i}{}^2(E,x).\overline{\phi_{i-1}}(E,x) \end{aligned} \tag{2.2}$$

Here, $\overline{\Phi}_{i-1}(E,x)$ and $S_{N(i-1)}(E,x)$ are mean quanta number and NPS incident on i^{th} stage. $\overline{g}_i(E,x)$ and $\sigma_{gi}^2(E, x)$ are mean gain and variance of gain in i^{th} stage. E is the incident X-ray photon energy. The first term in equation (2.2) represents the amplification of the quantum noise and the second term represents an additional noise due to the random fluctuation of the amplification gain of the i^{th} stage.

Stochastic blurring: Stochastic blurring is caused by random scattering of quanta in a distribution. Each quanta is randomly relocated to a new position with a certain probability. For the stochastic blurring stage *i*, output mean signal quanta per unit area and NPS are given by,

$$\begin{aligned} \overline{\phi_i}(E,x) &= \overline{\phi_{i-1}}(E,x).MTF_i(E,x) \\ S_{N_i}(E,x) &= \left[S_{N_{i-1}}(E,x) - \overline{\phi}_{i-1}(E,x) \right].MTF^2{}_i(E,x) + \overline{\phi}_{i-1}(E,x) \end{aligned} \tag{2.3}$$

Where $MTF_i(E,x)$ is the modulation transfer function of stage *i*.

Deterministic blurring: For the deterministic blurring stage *i*, output mean signal quanta per unit area and NPS are given by,

$$\overline{\phi_i}(E,x) = \overline{\phi_{i-1}}(E,x).MTF_i(E,x)$$

$$S_{N_i}(E,x) = \left[S_{N_{i-1}}(E,x) \right].MTF^2{}_i(E,x) \tag{2.4}$$

Chapter 3: Modeling of Detective Quantum Efficiency

3.1 Introduction

The concept of conventional X-ray photoconductor is well known, where the semiconductor is sandwiched between two charge collecting electrodes. The thicker photoconductor ensures the higher possibility of the absorption of incident quanta, hence increase of quantum efficiency. At the same time, it ensures higher sensitivity. But at the same time some new problems arise. Higher thickness contributes to more noise and signal spreading to the signal, as the carriers must travel longer distance to reach the charge collecting electrodes. At the same time, the possibility of charge trapping increases. All these causes reduction of charge collection efficiency, hence detective quantum efficiency (DQE) reduces.

To address this problem, a new model is introduced named folded device structure. In this structure, the direction of photon incident is parallel to the electrode. It is possible to increase the thickness of the detector to increase quantum efficiency, because the electrode distance can remain the same. So, quantum efficiency can be increased while maintaining charge collection efficiency, thus the detective quantum efficiency (DQE) increases.

In this chapter, the detective quantum efficiency (DQE) is modeled for both conventional and folded structure using cascaded linear system model. Cascaded linear system model is useful here because it breaks down imaging system into simple and independent stages, hence every single term associated with detective quantum efficiency (DQE) can be determined separately.

At first, stochastic amplification is discussed with mathematical explanation, because some of the stages of cascaded model obtain this process. Then both conventional and folded device structures are described using cascaded linear system model. Every stage (such as X-ray attenuation, conversion gain, charge collection efficiency, electronic noise) of the linear models are discussed with proper mathematical expressions. The expression of DQE for both structures (conventional and folded) are derived in this chapter.

3.2 Theoretical model

Conventional Structure: In conventional structure, a photoconductor layer is sandwiched between two parallel plate electrodes. A bias voltage is applied between the electrodes to produce electric field.

The DQE performance of many imaging systems is analyzed using a cascaded linear system model, where the imaging system is described as cascade of simple and independent stages. The cascaded linear system model for calculating DQE of conventional structure is shown in figure 3.1. This consists of four stages: (1) X-ray attenuation, (2) the creation of EHPs (Conversion gain), (3) charge collection process, (4) the addition of electronic noise. The flowchart in figure 3.1 illustrates the signal and noise power of every stage. Here spatial spreading of signal and noise is not considered, so in this work, DQE analysis represents zero spatial frequency detective quantum efficiency (DQE).

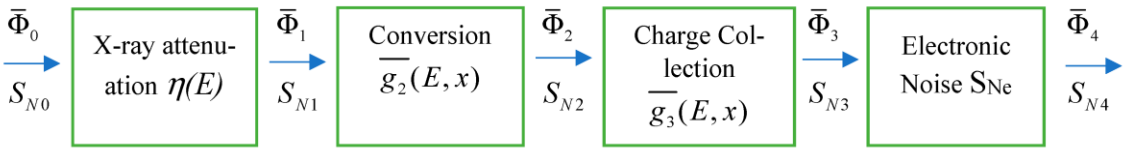

Figure 3.1: Cascaded linear system model for a conventional detector structure [34]

First three stages of the flowchart are defined as stochastic gain stage. For stochastic gain stage *i*, the output mean signal quanta and noise power spectrum (NPS) per unit area arising from incident X-ray photon interacts at x distance from radiation receiving electrodes are,

$$\begin{aligned} \overline{\phi_i}(E,x) &= \overline{g_i}(E,x).\overline{\phi_{i-1}}(E,x) \\ S_{N_i}(E,x) &= \overline{g_i}^2(E,x).S_{N_{i-1}}(E,x) + \sigma_{g_i}{}^2(E,x).\overline{\phi_{i-1}}(E,x) \end{aligned} \tag{3.1}$$

where E is incident photon energy, , $\overline{\Phi}_{i-1}(E,x)$ and $S_{N(i-1)}(E,x)$ are mean quanta number and NPS incident on i^{th} stage, $\bar{g}_i(E,x)$ and $\sigma_{gi}{}^2(E,x)$ are mean gain and variance of gain in i^{th} stage.

Now, from the flowchart from figure 3.1, the mean gain and variance of gain of each are determined as follows.

The gain of the X-ray attenuation stage is the quantum efficiency η of the detector, which is given by,

$$\eta(E) = 1 - e^{-\alpha d} \tag{3.2}$$

where E is the incident X-ray photon energy, $\alpha(E)$ and d are the linear attenuation coefficient and the distance between two electrodes (which is the same as the photoconductor layer thickness), respectively. An incident X-ray photon on this selection stage either interacts with the detector, probability η, or does not, probability $(1 - \eta)$. Therefore, this is a binary selection process [35]. According to the binomial theorem, the variance of η,

$$\sigma_{g1}^2 = \eta(1-\eta) \tag{3.3}$$

The mean conversion gain $\bar{g}_2(E,x)$ of the second stage represents the mean number of EHPs generated after the absorption of an X-ray photon interaction at x is,

$$\bar{g}_2(E,x) = \frac{E_{ab}(E,x)}{W_i} \tag{3.4}$$

where $E_{ab}(E, x)$ is the average absorbed energy per X-ray photon of energy E. For a relatively thinner detector, the reabsorption probability of the secondary photons is small and thus $E_{ab}(E) \approx (\alpha_{en}/\alpha)E$, where α_{en} is the energy absorption coefficient of the photoconductor. On the other hand, the secondary photons are mostly reabsorbed in a thicker detector (i.e., in detectors with high η) and thus, $E_{ab} \approx E$.

There is a fluctuation in conversion gain due to the stochastic fluctuation of the number of EHP generation per X-ray photon. We assume that the mean number of free EHPs released per X-ray photon obeys a Poisson process, i.e., $\sigma_{g_2}^2(E) \approx \bar{g}_2(E)$ [33][36].

The electric field remains relatively uniform across the photoconductor layer and bimolecular recombination is negligible in small signals, which is quite appropriate for medical diagnostic

applications [37]. The diffusion of carriers is negligible compared with their drift counterpart because of relatively high applied fields across the photoconductor. The general transport behavior in many photoconductors can be described in terms of a constant drift mobility μ and a single carrier lifetime τ for each type of carriers (holes and electrons) [33]. With these assumptions above, the average charge collection efficiency, $\bar{g}_3(x)$, at the electrodes from EHP generation at coordinate x can be written as [38],

$$\bar{g}_3(x) = x_t(1-e^{-\frac{x}{dx_t}}) + x_b(1-e^{-\frac{d-x}{dx_b}}) \tag{3.5}$$

where $x_t = \mu_t\tau_t F/d$, $x_b = \mu_b\tau_b F/d$. The subscript t and b refer to carrier types drifting to the top and bottom electrodes respectively; the top electrode receives the X-ray radiation. The variance of charge collection due to random trapping for an EHP generation at x is given by [39],

$$\sigma_{g_3}{}^2(x) = x_t{}^2 + x_b{}^2 - x_t{}^2 e^{-\frac{2x}{dx_t}} - x_b{}^2 e^{-\frac{2(d-x)}{dx_b}} - 2x_t\frac{x}{d}e^{-\frac{x}{dx_t}} - 2x_b(1-\frac{x}{d})e^{-\frac{d-x}{dx_b}} \tag{3.6}$$

During image readout, the image signal passes through TFT/CMOS switch and charge amplifiers and thus the equivalent electronic noise power S_{Ne} associated with these electronic components is added to the total noise power [40].

The input noise in the number of X-ray quanta incident on the detector is usually considered to follow a Poisson process and thus the input NPS is $S_{N0} = \bar{\Phi}_0$, where $\bar{\Phi}_0$ is the mean number of incident X-ray photons per unit area. Thus, the square of signal to noise ratio at the input,

$$\mathrm{SNR}_{\mathrm{in}}^2 = \bar{\Phi}_0 \tag{3.7}$$

In conventional structure (Figure 2.1), when X-ray photon interact with the material at a distance x from the top electrode, the probability density function of photon is expressed by following equation,

$$p_x(x) = c\exp(-\alpha x) \tag{3.8}$$

Where c is a constant, α is linear attenuation coefficient of the material. The following equation can be used to find the value of constant c,

$$\int_0^d c\exp(-\alpha x)dx = 1 \tag{3.9}$$

where *d* denotes photoconductor thickness. After solving the equation,

$$c = \frac{\alpha}{\eta} \tag{3.10}$$

Here η is quantum efficiency. This is expressed by following equation,

$$\eta = 1 - \exp(-\alpha d) \tag{3.11}$$

The X-rays are attenuated exponentially across the photoconductor thickness. Therefore, the probability density function for an X-ray photon, that is attenuated within a detector, to interact at a distance *x* from the top electrode is, [40],

$$P_x(x) = \frac{\alpha}{\eta} e^{-\alpha x} \qquad ;0 \le x \le d \tag{3.12}$$

Applying Equations (3.1) successively, the expected total signal at the output of the third stage is,

$$\bar{\Phi}_3 = \eta\,\bar{\Phi}_0 \bar{g}_2 \int_0^d \bar{g}_3(x)\, p_x(x)\, dx = \eta\,\bar{\Phi}_0 \bar{g}_2 \bar{\eta}_{cc} \tag{3.13}$$

where the average charge collection efficiency,

$$\bar{\eta}_{cc} = x_t \left\{ 1 - \frac{1 - e^{-\frac{1}{\Delta} - \frac{1}{x_t}}}{\left(1 - e^{-\frac{1}{\Delta}}\right)\left(1 + \frac{\Delta}{x_t}\right)} \right\} + x_b \left\{ 1 + \frac{e^{-\frac{1}{x_b}} - e^{-\frac{1}{\Delta}}}{\left(1 - e^{-\frac{1}{\Delta}}\right)\left(\frac{\Delta}{x_b} - 1\right)} \right\} \tag{3.14}$$

Similarly, the NPS at the output of third stage is,

$$S_{N3} = \bar{\Phi}_0 \eta \bar{g}_2 \int_0^d \left\{ \bar{g}_3^2(x)\left[1+\bar{g}_2\right] + {\sigma_{g_3}}^2(x) \right\} P_x(x)dx \tag{3.15}$$

$$\begin{aligned} S_{N3} &= \eta \bar{\Phi}_0 \bar{g}_2 \left(\bar{g}_2+1\right)\left[{x_t}^2(1+x_t A) + 2x_t x_b B + {x_b}^2\left(1+x_b C\right)\right] \\ &+\eta \bar{\Phi}_0 \bar{g}_2 \left[{x_t}^2\left(1+D\right) + {x_b}^2\left(1+E\right) + {x_t}^3 F + {x_b}^3 G\right] \end{aligned} \tag{3.16}$$

where,

$$A = 2\eta_a(e^{-\frac{1}{x_t}-\frac{1}{\Delta}}-1) - \eta_b(e^{-\frac{2}{x_t}-\frac{1}{\Delta}}-1),$$

$$B = 1 + x_t\eta_a\left(e^{-\frac{1}{x_t}-\frac{1}{\Delta}}-1\right) - x_b\eta_c\left(e^{-\frac{1}{\Delta}}-e^{-\frac{1}{x_b}}\right) + x_t x_b \eta_e\left(e^{-\frac{1}{x_t}-\frac{1}{\Delta}}-e^{-\frac{1}{x_b}}\right),$$

$$C = \eta_d\left(e^{\frac{1}{\Delta}}-e^{-\frac{2}{x_b}}\right) - 2\eta_c\left(e^{-\frac{1}{\Delta}}-e^{-\frac{1}{x_b}}\right),$$

$$D = 2\eta_a e^{-\frac{1}{x_t}-\frac{1}{\Delta}},$$

$$E = 2\eta_c e^{-\frac{1}{x_b}},$$

$$F = \eta_b\left(e^{-\frac{2}{x_t}-\frac{1}{\Delta}}-1\right) - 2\eta_f\left(1-e^{-\frac{1}{x_t}-\frac{1}{\Delta}}\right),$$

$$G = -\eta_d\left(e^{-\frac{1}{\Delta}}-e^{-\frac{2}{x_b}}\right) - 2\eta_g\left(e^{-\frac{1}{\Delta}}-e^{-\frac{1}{x_b}}\right),$$

$$\eta_a = \frac{1}{\eta\Delta\left(1+\frac{x_t}{\Delta}\right)}, \quad \eta_b = \frac{1}{\eta\Delta\left(2+\frac{x_t}{\Delta}\right)},$$

$$\eta_c = \frac{1}{\eta\Delta\left(1-\frac{x_b}{\Delta}\right)}, \quad \eta_d = \frac{1}{\eta\Delta\left(2-\frac{x_b}{\Delta}\right)},$$

$$\eta_e = \frac{1}{\eta\Delta\left(x_t - x_b - \frac{x_t x_b}{\Delta}\right)},$$

$$\eta_f = \frac{1}{\eta\Delta\left(1+\frac{x_t}{\Delta}\right)^2},$$

$$\eta_g = \frac{1}{\eta\Delta\left(1-\frac{x_b}{\Delta}\right)^2}.$$

Using Equation (2.1), the DQE at the output of the detector is

$$\mathrm{DQE} = \frac{\bar{\Phi}_3^2}{\bar{\Phi}_0\left(S_{N3} + S_{Ne}\right)} \tag{3.17}$$

Folded Structure: In folded structure, the direction of photon incident is parallel to the electrodes. It is possible to increase the thickness of detector to increase the quantum efficiency, because the distance between the electrodes can be maintained. As a result, unlike conventional structure, increase of quantum efficiency (increase in device thickness) does not reduce the charge collection efficiency, hence the overall DQE increases.

The quantum efficiency for the folded structure can be expressed as

$$\eta(E) = 1 - e^{-\alpha(E)l} \tag{3.18}$$

where l is photoconductor thickness.

The cascaded linear system model for calculating DQE of a folded structure has an additional stochastic gain stage, named as "effective filling" as shown in Figure 3.2.

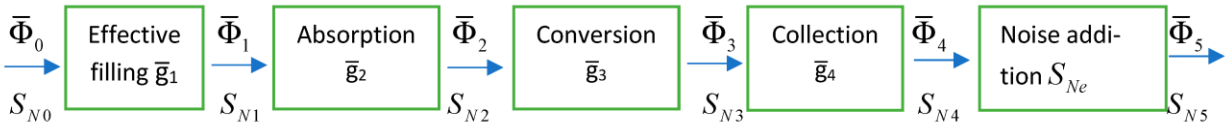

Figure 3.2: Cascaded linear system model for the folded structure [34]

The X-ray absorption in the electrode volume does not contribute to the EHP generation and this loss can be determined by the effective fill factor [41],

$$\bar{g}_1 = \frac{d}{d + d_{foil}} \tag{3.19}$$

where the width of the electrode is d_{foil}. The gain of this stage is g_1. Assuming a binomial selection process [29], the variance of gain $\sigma_{g1}^2 = \bar{g}_1\left(1 - \bar{g}_1\right)$.

Equations (3.5) and (3.6) are applicable for calculating the average charge collection $\bar{g}_4\left(x\right)$ and the variance of charge collection $\sigma_4^2\left(x\right)$ at the electrodes from EHP generation at coordinate *x*.

For folded structure (Figure 2.2), X-ray photons incident on the semiconductor material parallel to electrodes. Let's consider, the photon interacts with the material at a distance y from the surface. Then through direct conversion, electron hole pairs are generated, and they drift in opposite direction due to the electric field. The drifting direction of electron and hole is perpendicular with the direction of photon injection. The probability density of X-ray photon for folded structure is described as

$$p_{x,y}(y) = c\exp(-\alpha y)$$

Where c is a constant and α is linear attenuation coefficient. The following equation can be used to find the value of constant c,

$$\int_0^d \int_0^l c\exp(-\alpha y)dydx = 1$$

Where l is the thickness of photoconductor, and d is the distance between two electrodes. After solving this equation,

$$c = \frac{\alpha}{\eta d}$$

η is quantum efficiency. It is expressed as

$$\eta = 1 - \exp(-\alpha l)$$

So, the probability density function per unit area for an X-ray photon to interact at a distance y from the top electrode is,

$$p_{xy}(y) = \frac{\alpha}{\eta d} e^{-\alpha y} \qquad ; 0 \le y \le l \tag{1.20}$$

The total output signal after fourth stage,

$$\bar{\Phi}_4 = \eta \bar{\Phi}_0 \bar{g}_1 \bar{g}_3 \int_0^d \int_0^l \bar{g}_4(x)\, p_{xy}(y)\, dydx = \eta \bar{\Phi}_0 \bar{g}_1 \bar{g}_3 \bar{\eta}_{cc} \tag{3.21}$$

where,

$$\bar{\eta}_{cc} = (x_t + x_b) - x_t^2 \left(1 - e^{-\frac{1}{x_t}}\right) - x_b^2 \left(1 - e^{-\frac{1}{x_b}}\right) \tag{3.22}$$

The NPS at the output of fourth stage is,

$$S_{N4} = \bar{\Phi}_0 \eta \bar{g}_1 \bar{g}_3 \int_0^d \int_0^l \left\{ \bar{g}_4^2(x)\left[1 + \bar{g}_3\right] + \sigma_{g_4}{}^2(x) \right\} p_{xy}(y) dydx \tag{3.23}$$

$$S_{N4} = \bar{g}_3\bar{g}_1\bar{\Phi}_0\eta\left(1+\bar{g}_3\right)\left[\begin{array}{l} x_t{}^2\left\{1+2x_t\left(e^{-\frac{1}{x_t}}-1\right)-\frac{x_t}{2}\left(e^{-\frac{2}{x_t}}-1\right)\right\} \\ +2x_tx_b\left\{1+x_t\left(e^{-\frac{1}{x_t}}-1\right)-x_b\left(1-e^{-\frac{1}{x_b}}\right)+\frac{x_tx_b}{x_t-x_b}\left(e^{-\frac{1}{x_t}}-e^{-\frac{1}{x_b}}\right)\right\} \\ +x_b{}^2\left\{1-2x_b\left(1-e^{-\frac{1}{x_b}}\right)+\frac{x_b}{2}\left(1-e^{-\frac{2}{x_b}}\right)\right\} \end{array}\right] \tag{3.24}$$

$$+\bar{g}_3\bar{g}_1\eta\bar{\Phi}_0\left[\begin{array}{l} x_t{}^2\left\{1+\frac{x_t}{2}\left(e^{-\frac{2}{x_t}}-1\right)+2e^{-\frac{1}{x_t}}+2x_t\left(e^{-\frac{1}{x_t}}-1\right)\right\} \\ +x_b{}^2\left\{1+\frac{x_b}{2}\left(e^{-\frac{2}{x_b}}-1\right)+2e^{-\frac{1}{x_b}}+2x_b\left(e^{-\frac{1}{x_b}}-1\right)\right\} \end{array}\right]$$

The DQE at the output (after fifth stage),

$$\mathrm{DQE} = \frac{\bar{\Phi}_4^2}{\bar{\Phi}_0\left(S_{N4}+S_{Ne}\right)} \tag{3.25}$$

Chapter 4: Results and Discussions

4.1 Introduction

In the previous chapter, mathematical models have been developed to determine the detective quantum efficiency (DQE) for both conventional and folded device structure of X-ray detector. In the model, the random trapping of charge carrier inside the semiconductor has been considered. At the same time, the spatial spreading of signal and noise through the semiconductor is not considered, so in this work, I will analyze zero spatial frequency detective quantum efficiency (DQE).

Based on cascaded linear system model, both detector structures will be investigated for fluoroscopy and mammography application. I will conduct study to obtain proper design specification of photodetector for these medical applications, and there will be a comparison between conventional and folded structure for the applications (fluoroscopy and mammography) based on their imaging performance. There will also be a comparative study to compare between amorphous selenium and poly-$MAPbI_3$ for both structures.

The equations in chapter 3 were used to plot graphs of DQE using software MATLAB. The effects of radiation intensity, carrier mobility, carrier lifetime, electronic noise, electric field on the DQE were analyzed quantitatively.

4.2 Perovskite X-ray Detectors

The DQE performance of poly-$MAPbI_3$ detector having folded and conventional structures was evaluated for both fluoroscopy and mammography applications. The thickness of the electrode in the folded structure is assumed to be d_{foil}=2.8μm. The electric field is considered to be F = 1 V/μm. The average photon energies are assumed to be 60 keV and 20 keV for fluoroscopy and mammographic applications, respectively. We have considered ambipolar charge transport assuming equal electron and hole mobilities [42][43][44]. The carrier transport properties (mobility and lifetime) of electrons and holes are very similar in poly-$MAPbI_3$ [45]. In the simulation, we have varied the $\mu\tau$ values from 10^{-5} cm^2/V cm^2/V to 10^{-7} cm^2/V, which are reasonable for poly-$MAPbI_3$ [23]. While calculating detective quantum efficiency, different

ranges of exposure are used for different applications. The range of exposure varies from 0.1 to 10 μR with the mean exposure being 1 μR in Fluoroscopy application where it varies from 0.6 to 240 mR with the mean exposure being 12 mR in mammography application [46]. Several sources of electronic noise are associated with the read-out technology. TFT reset noise or kTC noise (typical value is 600 *e*) is the dominant sources of electronic noise, data line and charge amplifier noise (typical value is 800–2000 *e* in passive pixel) per pixel also plays a big role. The total noise power is the sum of the noise power of all the sources, and each of the component sources of noise is independent. The pixel size for fluoroscopic image sensors is large and the total electronic noise (N_e) typically varies from 1000 e to 2000 e per pixel whereas it varies from 500 *e* to 1000 *e* per pixel in mammographic detectors due to their smaller pixel size and the use of CMOS or active pixel technology [23]. The noise power, $S_{Ne} = N_e^2$.

4.2.1: Folded Structure (Fluoroscopy)

The effect of electric field, exposure, carrier density, electronic noise on DQE were studied for fluoroscopy. For fluoroscopy application, pixel area is 200 μm × 200 μm.

When noise=1000e and Photon energy=60keV

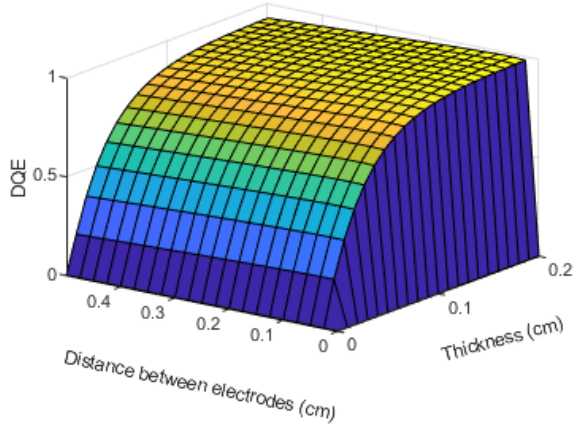

(a)

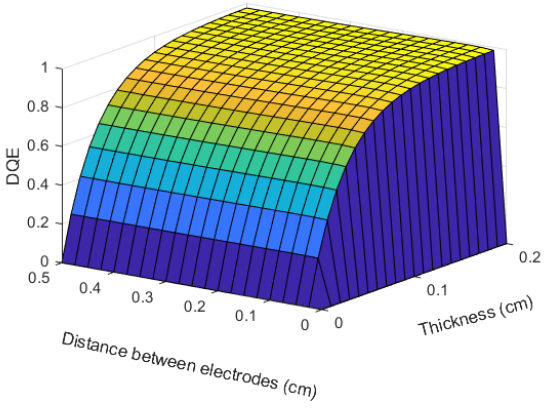

(b)

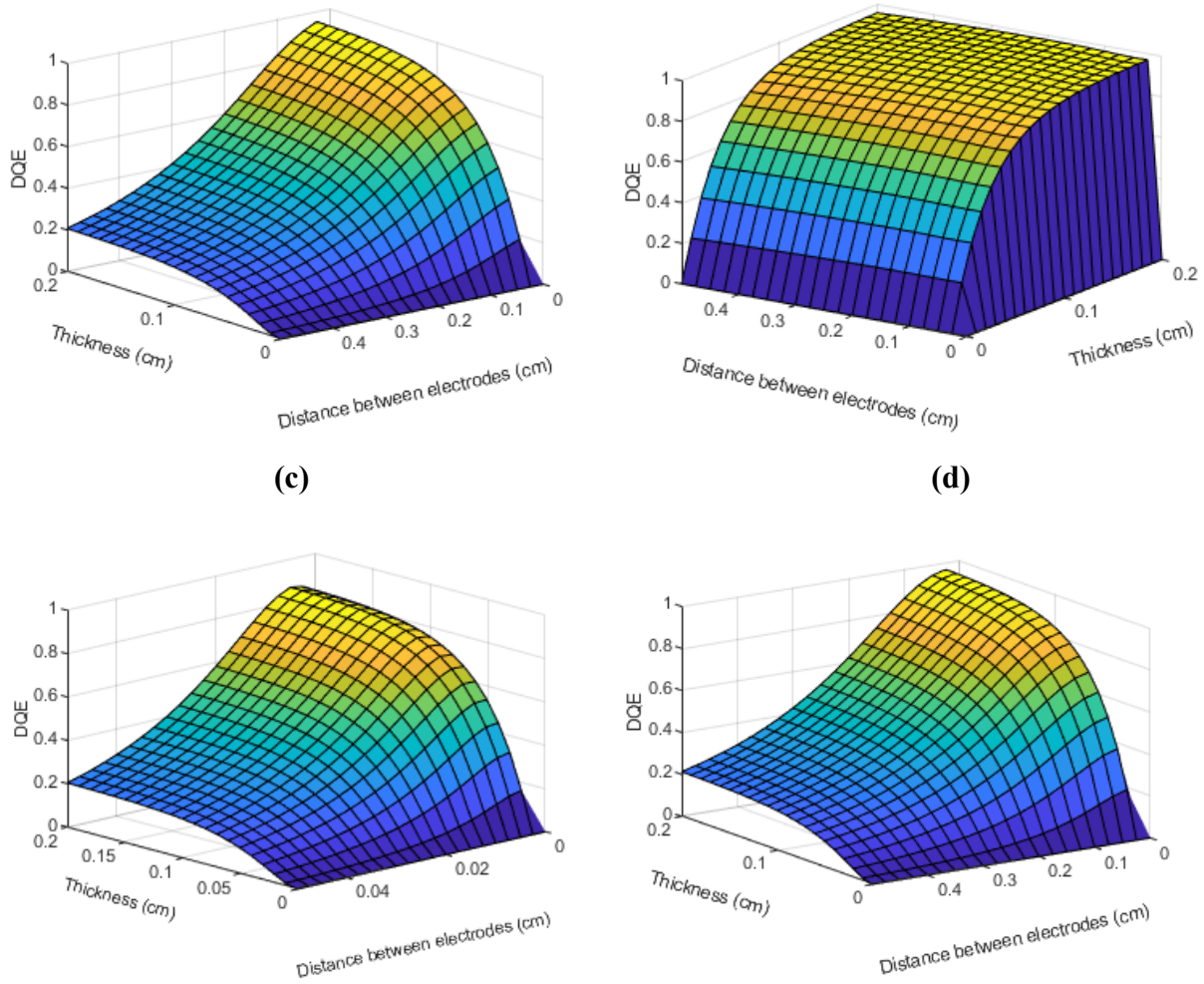

Figure 4.1: Fluoroscopy application for folded poly-$MAPbI_3$ X-ray detector. Detective quantum efficiency (DQE) as a function of photoconductor thickness l and distance between electrodes d. (a) photon energy E=60keV, $\mu\tau= 10^{-5}$ cm^2/V, exposure X=0.1μR, Electronic noise Ne=1000e, (b) photon energy E=60keV, $\mu\tau= 10^{-5}$ cm2/V, exposure X=10μR, Electronic noise Ne=1000e, (c) photon energy E=60keV, $\mu\tau= 10^{-6}$ cm^2/V, exposure X=0.1μR, Electronic noise Ne=1000e, (d) photon energy E=60keV, $\mu\tau= 10^{-6}$ cm^2/V, exposure X=10μR, Electronic noise Ne=1000e, (e) photon energy E=60keV, $\mu\tau= 10^{-7}$ cm^2/V, exposure X=0.1μR, Electronic noise Ne=1000e, (f) photon energy E=60keV, $\mu\tau= 10^{-7}$ cm^2/V, exposure X=10μR, Electronic noise Ne=1000e.

Figure 4.1 shows the affect of change in photoconductor thickness *l* and electrode distance *d* on DQE for fluoroscopy application in folded structure. The applied electric field was F=1 V/μm and incident photon energy was E=60keV. The nominal exposure of X=0.1μR was used in figure 4.1a, 4.1c, 4.1e, and X=10μR was used for figure 4.1b, 4.1d, 4.1f. The electron hole pair (EHP) creation energy $W_{\pm}$ was 5eV [29]. Electronic noise was 1000e. The multiplication of carrier

mobility and lifetime was considered same for both electron and hole, which was $\mu\tau = 10^{-5}$ cm^2/V in figure 4.1a and 4.1b, $\mu\tau = 10^{-6}$ cm^2/V in figure 4.1c and 4.1d, and $\mu\tau = 10^{-7}$ cm^2/V in figure 4.1e and 4.1f, respectively.

In figure 4.1a, 4.1b, and 4.1d, the DQE increases with the increase in photoconductor thickness gradually. At the same time, at first DQE increases with the increase in distance between the charge collecting electrodes, and after reaching a certain value of *d* (distance between electrode), DQE reaches its maximum value (more than 0.9 for all three curves), then starts to decrease.

In figure 4.1c, 4.1e, and 4.1f, at first DQE increases almost linearly with the increase of photoconductor thickness. Then the DQE increases slowly with increase in thickness. At the same time, at first DQE increases rapidly with the increase of distance between charge collecting electrodes. After reaching the pick value (more than 0.8), DQE starts to decrease with the increase of distance between electrodes.

When noise=2000e and Photon energy=60keV

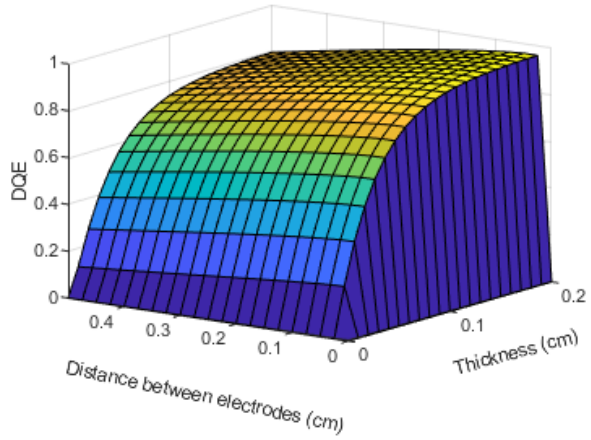

(a)

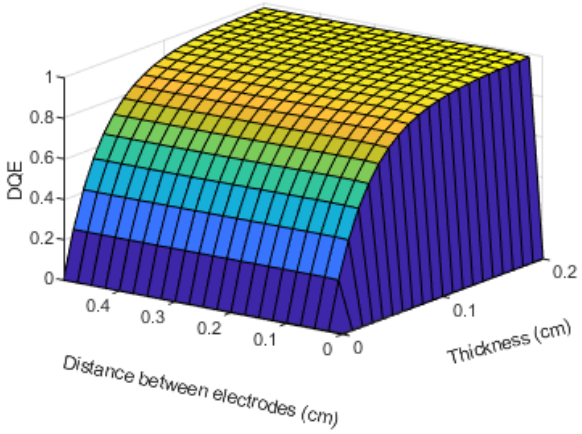

(b)

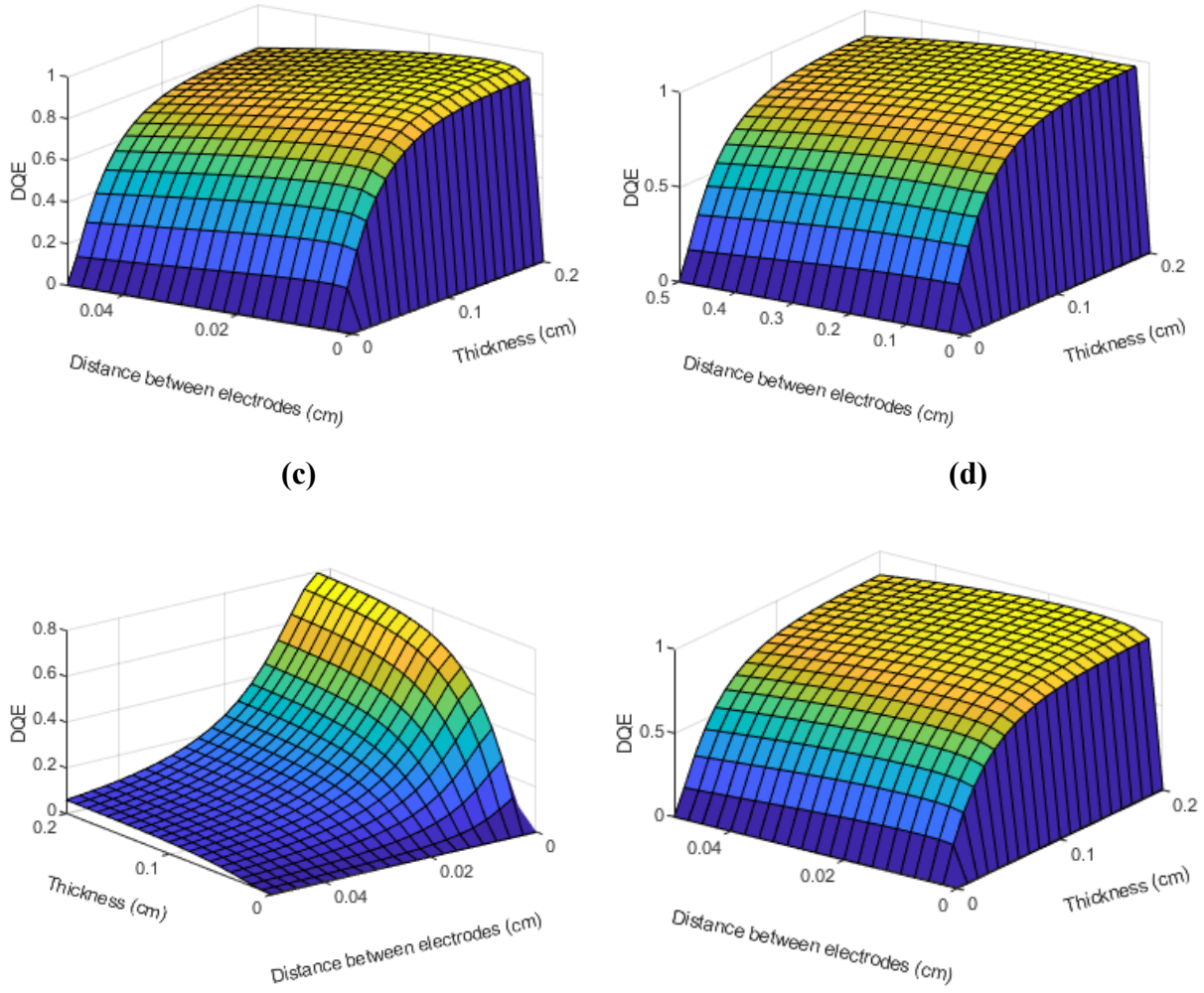

Figure 4.2: Fluoroscopy application for folded poly-$MAPbI_3$ X-ray detector. Detective quantum efficiency (DQE) as a function of photoconductor thickness l and distance between electrodes d.
(a) photon energy E=60keV, $\mu\tau = 10^{-5}$ cm^2/V, exposure X=0.1μR, Electrical noise Ne=2000e
(b) photon energy E=60keV, $\mu\tau = 10^{-5}$ cm^2/V, exposure X=10μR, Electrical noise Ne=2000e
(c) photon energy E=60keV, $\mu\tau = 10^{-6}$ cm^2/V, exposure X=0.1μR, Electrical noise Ne=2000e
(d) photon energy E=60keV, $\mu\tau = 10^{-6}$ cm^2/V, exposure X=10μR, Electrical noise Ne=2000e
(e) photon energy E=60keV, $\mu\tau = 10^{-7}$ cm^2/V, exposure X=0.1μR, Electrical noise Ne=2000e
(f) photon energy E=60keV, $\mu\tau = 10^{-7}$ cm^2/V, exposure X=10μR, Electrical noise Ne=2000e

Figure 4.2 shows the affect of change in photoconductor thickness *l* and electrode distance *d* on DQE for fluoroscopy application in folded structure. The applied electric field was F=1 V/μm and incident photon energy was E=60keV. The nominal exposure of X=0.1μR was used in figure 4.2a, 4.2c, 4.2e, and X=10μR was used for figure 4.2b, 4.2d, 4.2f. The electron hole pair (EHP)

creation energy $W_{\pm}$ was 5eV [29]. Electronic noise was 2000e. The multiplication of carrier mobility and lifetime was considered same for both electron and hole, which was $\mu\tau = 10^{-5}$ cm^2/V in figure 4.2a and 4.2b, $\mu\tau = 10^{-6}$ cm^2/V in figure 4.2c and 4.2d, and $\mu\tau = 10^{-7}$ cm^2/V in figure 4.2e and 4.2f, respectively.

In figure 4.2a, 4.2b, 4.2c, 4.2d, and 4.2f, the detective quantum efficiency (DQE) curve shows increasing tendency with the increase of photoconductor thickness. At the same time, at first DQE increases with the increase in distance between charge collecting electrodes very rapidly, and after reaching a certain value of *d* (distance between electrode), DQE reaches its maximum value (more than 0.8 for every case), and then it starts to decrease.

In figure 4.2e, at first DQE increases almost linearly with the increase of photoconductor thickness. When the thickness is more than 0.1cm, DQE increases slowly with increase in thickness. At the same time, at first DQE increases rapidly with the increase of distance between charge collecting electrodes. After reaching its pick value (0.8), DQE starts to decrease with increase of the distance between electrodes.

4.2.2: Folded Structure (Mammography)

The effect of electric field, exposure, carrier density, electronic noise on DQE were studied for mammography. For mammography application, pixel area is 50 μm × 50 μm.

When noise=500e and Photon energy=20keV

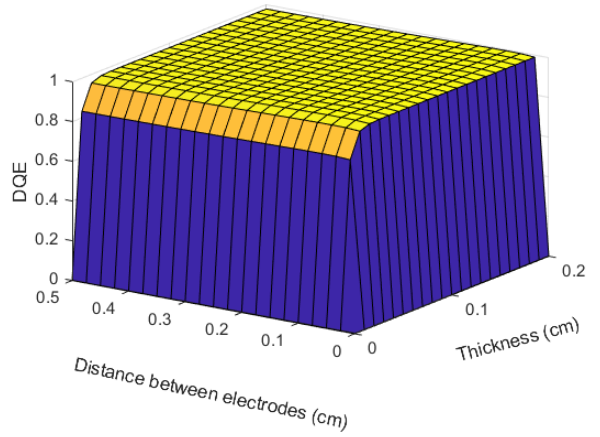

(a)

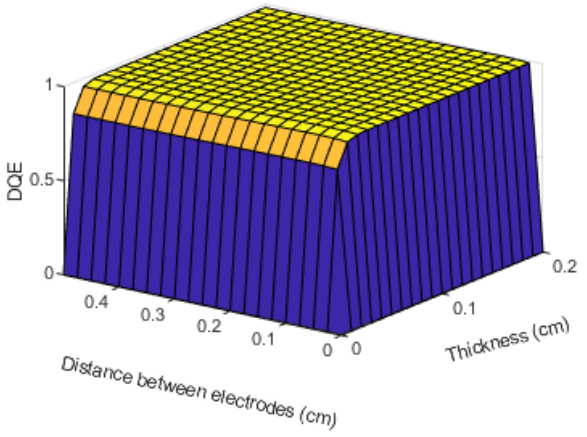

(b)

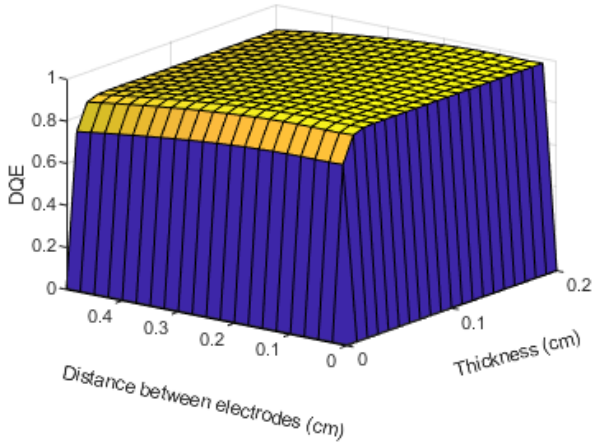

(c)

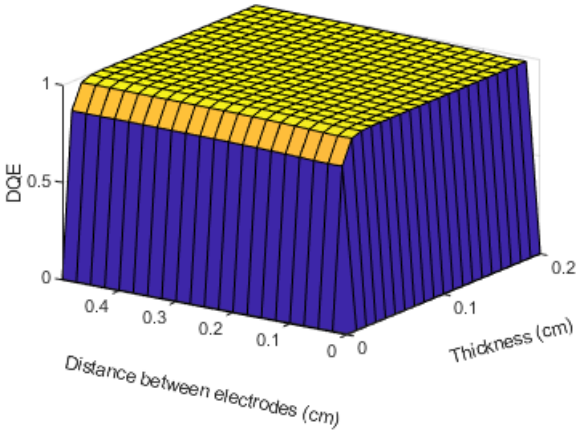

(d)

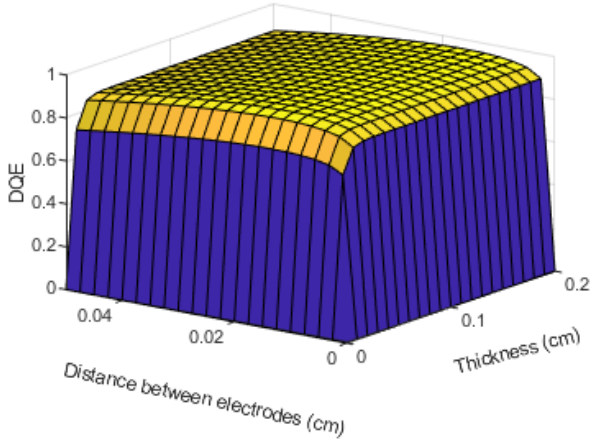

(e)

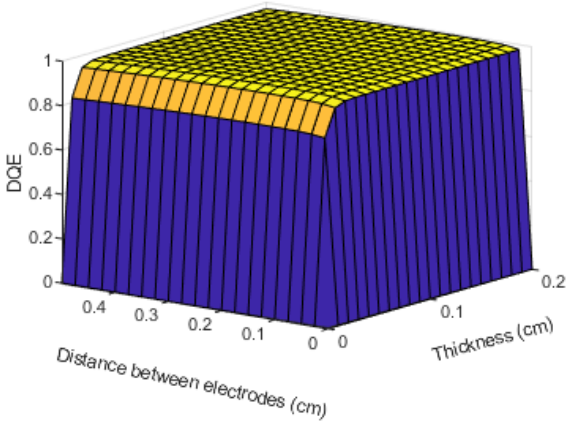

(f)

Figure 4.3: Mammography application for folded poly-$MAPbI_3$ X-ray detector. Detective quantum efficiency (DQE) as a function of photoconductor thickness l and distance between electrodes d.

(a) Photon energy E=20keV, $\mu\tau= 10^{-5}$ cm^2/V, exposure X=0.6mR, Electrical noise Ne=500e
(b) Photon energy E=20keV, $\mu\tau= 10^{-5}$ cm^2/V, exposure X=240mR, Electrical noise Ne=500e
(c) Photon energy E=20keV, $\mu\tau= 10^{-6}$ cm^2/V, exposure X=0.6mR, Electrical noise Ne=500e
(d) Photon energy E=20keV, $\mu\tau= 10^{-6}$ cm^2/V, exposure X=240mR, Electrical noise Ne=500e
(e) Photon energy E=20keV, $\mu\tau= 10^{-7}$ cm^2/V, exposure X=0.6mR, Electrical noise Ne=500e
(f) Photon energy E=20keV, $\mu\tau= 10^{-7}$ cm^2/V, exposure X=240mR, Electrical noise Ne=500e

Figure 4.3 shows the affect of change in photoconductor thickness *l* and electrode distance *d* on DQE for mammography application in folded structure. The applied electric field was F=1 V/μm and incident photon energy was E=20keV. The nominal exposure of X=0.6mR was used in figure 4.3a, 4.3c, 4.3e, and X=240mR was used for figure 4.3b, 4.3d, 4.3f. The electron hole pair (EHP) creation energy $W_{\pm}$ was 5eV [29]. Electronic noise was 500e. The multiplication of carrier mobility and lifetime was considered same for both electron and hole, which was $\mu\tau= 10^{-5}$ cm^2/V in figure 4.3a and 4.3b, $\mu\tau= 10^{-6}$ cm^2/V in figure 4.3c and 4.3d, and $\mu\tau= 10^{-7}$ cm^2/V in figure 4.3e and 4.3f, respectively.

In figure 4.3a, 4.3b, 4.3c, 4.3d, 4.3e, and 4.3f, the detective quantum efficiency (DQE) gradually increases with the increase of photoconductor thickness. At the same time, at first DQE shows increasing tendency with the increase in distance between charge collecting electrodes, and after reaching a certain value of *d* (distance between electrode), DQE reaches its maximum value (more than 0.9), then starts to decrease with the increase of distance between electrodes.

When noise=1000e and Photon energy=20keV

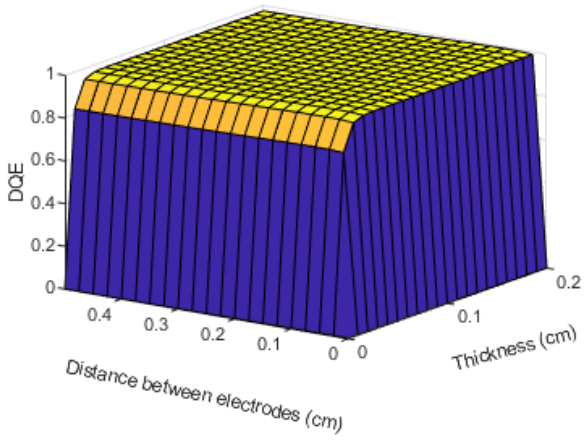

(a)

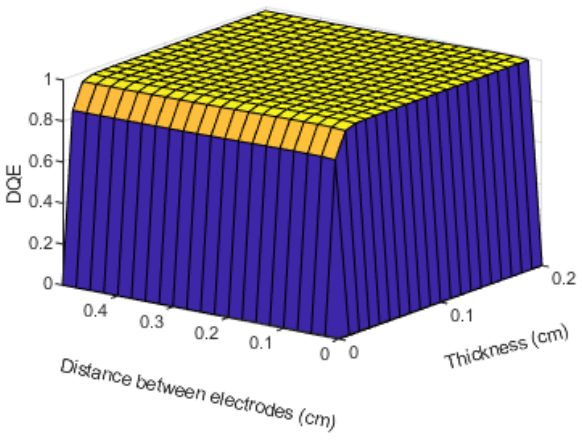

(b)

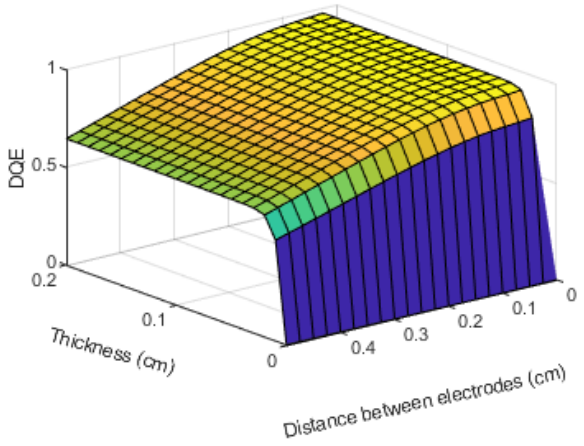

(c)

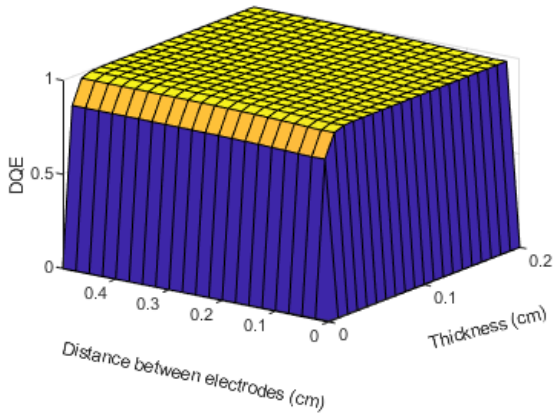

(d)

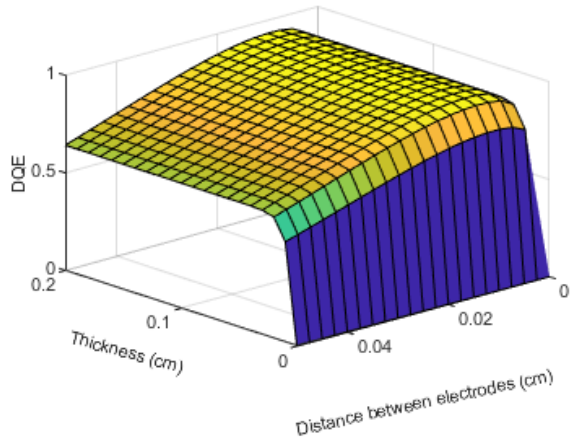

(e)

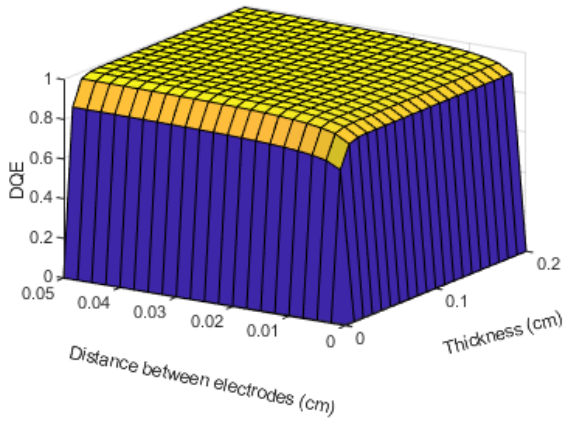

(f)

Figure 4.4: Mammography application for folded poly-$MAPbI_3$ X-ray detector. Detective quantum efficiency (DQE) as a function of photoconductor thickness l and distance between electrodes d. (a) photon energy E=20keV, $\mu\tau= 10^{-5}$ cm^2/V, exposure X=0.6mR, Electrical noise Ne=1000e, (b) photon energy E=20keV, $\mu\tau= 10^{-5}$ cm^2/V, exposure X=240mR, Electrical noise Ne=1000e, (c) photon energy E=20keV, $\mu\tau= 10^{-6}$ cm^2/V, exposure X=0.6mR, Electrical noise Ne=1000e, (d) photon energy E=20keV, $\mu\tau= 10^{-6}$ cm^2/V, exposure X=240mR, Electrical noise Ne=1000e, (e) photon energy E=20keV, $\mu\tau= 10^{-7}$ cm^2/V, exposure X=0.6mR, Electrical noise Ne=1000e, (f) photon energy E=20keV, $\mu\tau= 10^{-7}$ cm^2/V, exposure X=240mR, Electrical noise Ne=1000e

Figure 4.4 shows the affect of change in photoconductor thickness *l* and electrode distance *d* on DQE for mammography application in folded structure. The applied electric field was F=1 V/μm and incident photon energy was E=20keV. The nominal exposure of X=0.6mR was used in figure 4.4a, 4.4c, 4.4e, and X=240mR was used for figure 4.4b, 4.4d, 4.4f. The electron hole pair (EHP) creation energy $W_{\pm}$ was 5eV [29]. Electronic noise was 1000e. The multiplication of carrier mobility and lifetime was considered same for both electron and hole, which was $\mu\tau= 10^{-5}$ cm^2/V in figure 4.4a and 4.4b, $\mu\tau= 10^{-6}$ cm^2/V in figure 4.4c and 4.4d, and $\mu\tau= 10^{-7}$ cm^2/V in figure 4.4e and 4.4f, respectively.

In figure 4.4a, 4.4b, 4.4d, and 4.4f, at first the DQE increases with the increase of photoconductor thickness rapidly, and after reaching a certain thickness, DQE increases very slowly with increase of thickness. At the same time, at first DQE increases with the increase in distance between electrodes with large slopes, and after reaching a certain value of *d* (distance between electrode), DQE reaches its maximum value (more than 0.8) and decrease if *d* is increased further.

In figure 4.4c, and 4.4e, at first DQE increases almost linearly with the increase of photoconductor thickness. After reaching a certain thickness, DQE increases slowly if thickness is increased. At the same time, DQE increases rapidly with the increase of distance between charge collecting electrodes. After reaching the pick value, DQE starts to decrease with the increase of distance between electrodes.

4.2.3: Conventional Structure (Fluoroscopy)

The effect of electric field, exposure, carrier density, electronic noise on DQE were studied for fluoroscopy in conventional structure. For fluoroscopy application, pixel area is 200 µm × 200 µm.

When noise=1000e and Photon energy=60keV

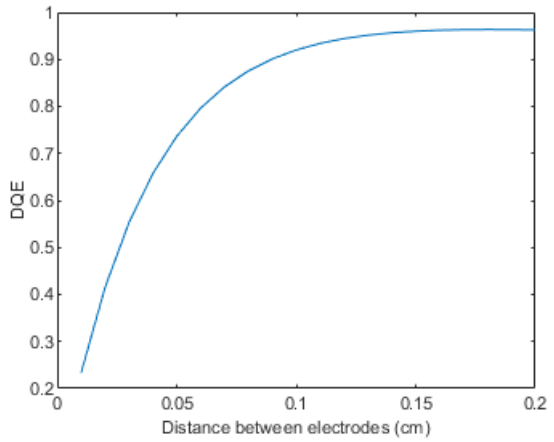

(a)

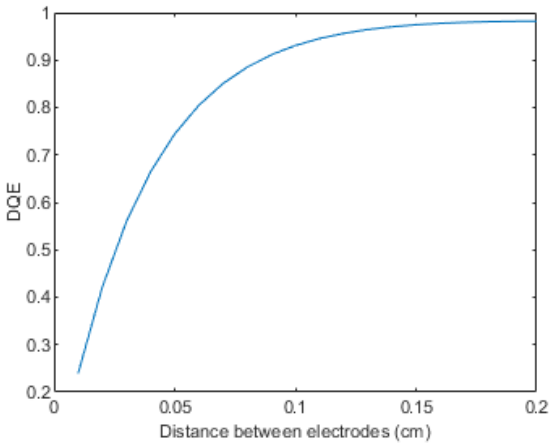

(b)

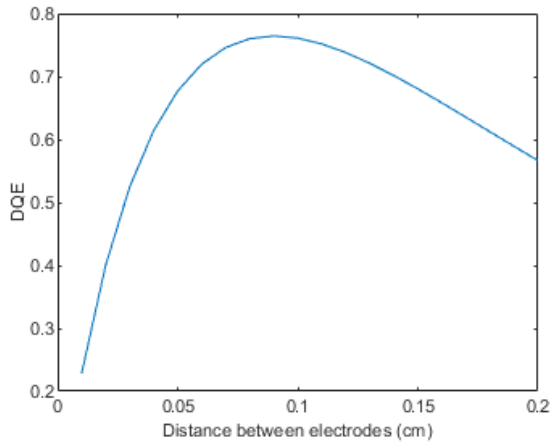

(c)

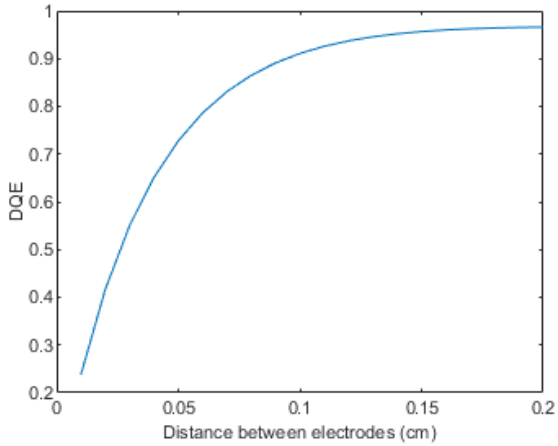

(d)

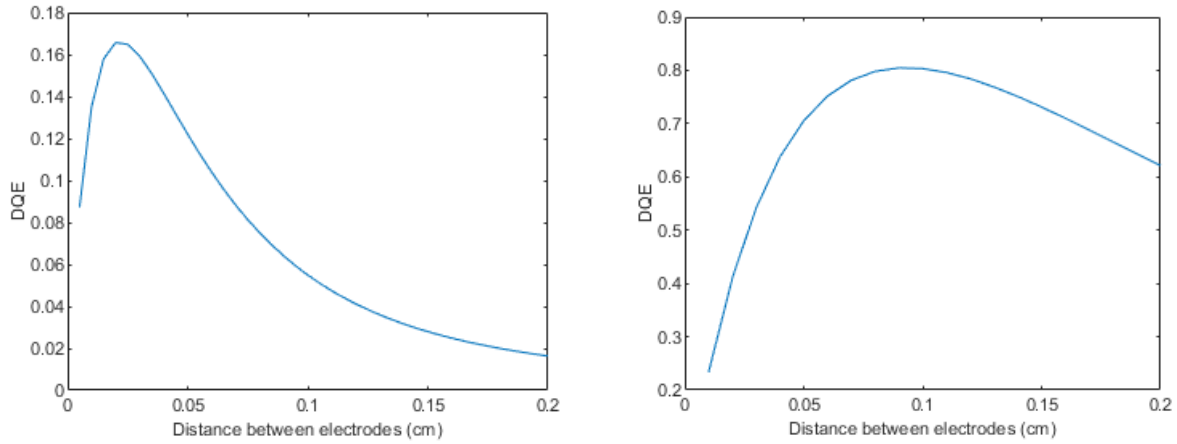

(e) **(f)**

Figure 4.5: Fluoroscopy application for conventional poly-$MAPbI_3$ X-ray detector. Detective quantum efficiency (DQE) as a function of photoconductor thickness d. (a) photon energy E=60keV, $\mu\tau= 10^{-5}$ cm^2/V, exposure X=0.1μR, Electrical noise Ne=1000e, (b) photon energy E=60keV, $\mu\tau= 10^{-5}$ cm^2/V, exposure X=10μR, Electrical noise Ne=1000e, (c) photon energy E=60keV, $\mu\tau= 10^{-6}$ cm^2/V, exposure X=0.1μR, Electrical noise Ne=1000e, (d) photon energy E=60keV, $\mu\tau= 10^{-6}$ cm^2/V, exposure X=10μR, Electrical noise Ne=1000e, (e) photon energy E=60keV, $\mu\tau= 10^{-7}$ cm^2/V, exposure X=0.1μR, Electrical noise Ne=1000e, (f) photon energy E=60keV, $\mu\tau= 10^{-7}$ cm^2/V, exposure X=10μR, Electrical noise Ne=1000e.

Figure 4.5 shows the affect of change in electrode distance *d* on DQE for fluoroscopy application in conventional structure. In conventional structure, distance between electrodes is considered as photoconductor thickness. The applied electric field was F=1 V/μm and incident photon energy was E=60keV. The nominal exposure of X=0.1μR was used in figure 4.5a, 4.5c, 4.5e, and X=10μR was used for figure 4.5b, 4.5d, 4.5f. The electron hole pair (EHP) creation energy $W_{\pm}$ was 5eV [29]. Electronic noise was 1000e. The multiplication of carrier mobility and lifetime was considered same for both electron and hole, which was $\mu\tau= 10^{-5}$ cm^2/V in figure 4.5a and 4.5b, $\mu\tau= 10^{-6}$ cm^2/V in figure 4.5c and 4.5d, and $\mu\tau= 10^{-7}$ cm^2/V in figure 4.5e and 4.5f, respectively.

In figure 4.5a, 4.5b, and 4.5d, DQE gradually increases with the increase of photoconductor thickness. Maximum DQE of about 0.9 is observed for them. In figure 4.5c and 4.5f, the DQE increases with the photoconductor thickness gradually, and after reaching the peak value (0.77 and 0.81 for figure 4.5c and 4.5f, respectively), DQE starts to drop slowly if thickness is

increased further. In figure 4.5e, DQE reaches the peak value (0.17) for thickness of 0.02cm, then it drops rapidly with increase of thickness between charge collecting electrodes.

When noise=2000e and Photon energy=60keV

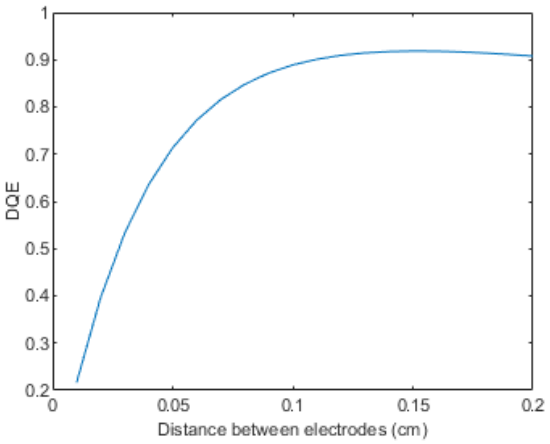

(a)

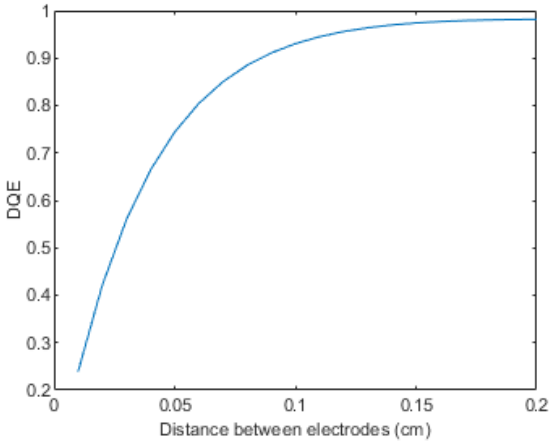

(b)

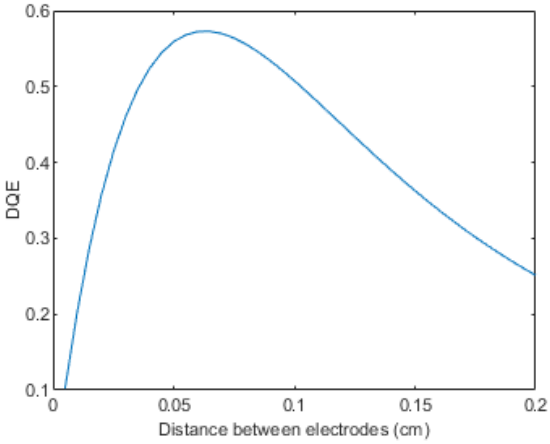

(c)

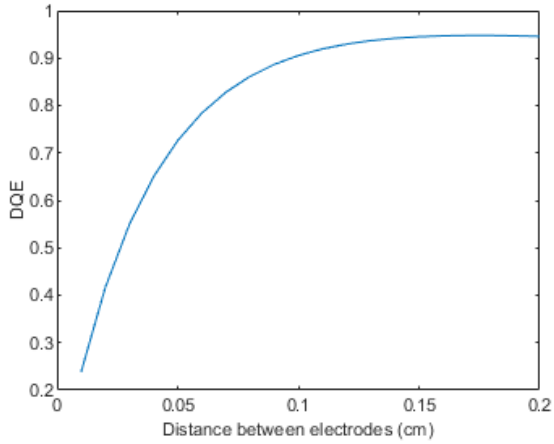

(d)

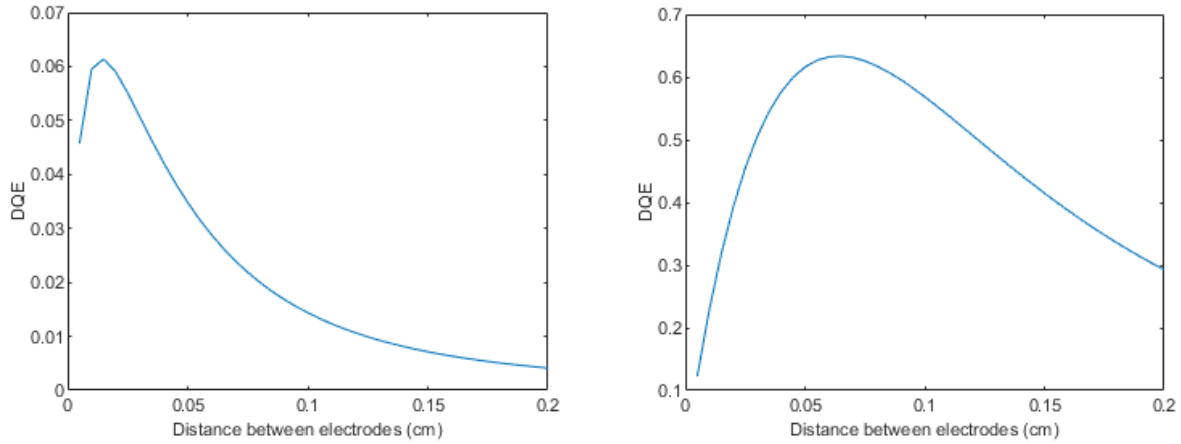

(e) **(f)**

Figure 4.6: Fluoroscopy application for conventional poly-$MAPbI_3$ X-ray detector. Detective quantum efficiency (DQE) as a function of photoconductor thickness d. (a) photon energy E=60keV, $\mu\tau= 10^{-5}$ cm^2/V, exposure X=0.1μR, Electrical noise Ne=2000e, (b) photon energy E=60keV, $\mu\tau= 10^{-5}$ cm^2/V, exposure X=10μR, Electrical noise Ne=2000e, (c) photon energy E=60keV, $\mu\tau= 10^{-6}$ cm^2/V, exposure X=0.1μR, Electrical noise Ne=2000e, (d) photon energy E=60keV, $\mu\tau= 10^{-6}$ cm^2/V, exposure X=10μR, Electrical noise Ne=2000e, (e) photon energy E=60keV, $\mu\tau= 10^{-7}$ cm^2/V, exposure X=0.1μR, Electrical noise Ne=2000e, (f) photon energy E=60keV, $\mu\tau= 10^{-7}$ cm^2/V, exposure X=10μR, Electrical noise Ne=2000e.

Figure 4.6 shows the affect of change in electrode distance *d* on DQE for fluoroscopy application in conventional structure. In conventional structure, distance between electrodes is considered as photoconductor thickness. The applied electric field was F=1 V/μm and incident photon energy was E=60keV. The nominal exposure of X=0.1μR was used in figure 4.6a, 4.6c, 4.6e, and X=10μR was used for figure 4.6b, 4.6d, 4.6f. The electron hole pair (EHP) creation energy $W_{\pm}$ was 5eV [29]. Electronic noise was 2000e. The multiplication of carrier mobility and lifetime was considered same for both electron and hole, which was $\mu\tau= 10^{-5}$ cm^2/V in figure 4.6a and 4.6b, $\mu\tau= 10^{-6}$ cm^2/V in figure 4.6c and 4.6d, and $\mu\tau= 10^{-7}$ cm^2/V in figure 4.6e and 4.6f, respectively.

In figure 4.6a, 4.6b, and 4.6d, detective quantum efficiency (DQE) gradually increases with the increase of photoconductor thickness and reaches up to 0.9. In figure 4.6c and 4.6f, the DQE increases with the photoconductor thickness gradually, and after reaching the peak value of DQE at a certain thickness (0.57 at 0.06cm and 0.62 at 0.06cm for figure 4.6c and 4.6f, respectively),

DQE starts to drop slowly if thickness is increased further. In figure 4.6e, DQE reaches the peak value (0.06) for thickness of 0.018cm, then it drops rapidly with increase of distance between charge collecting electrodes. Very poor imaging performance is observed for figure 4.6e.

4.2.4: Conventional Structure (Mammography)

The effect of electric field, exposure, carrier density, electronic noise on DQE were studied for mammography. For mammography application, pixel area is 50 μm × 50 μm.

When noise=500e and Photon energy=20keV

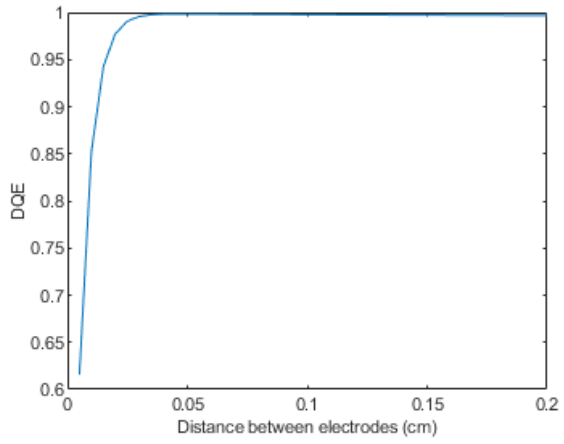

(a)

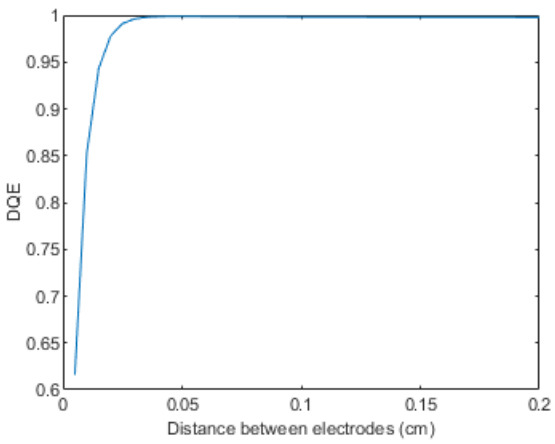

(b)

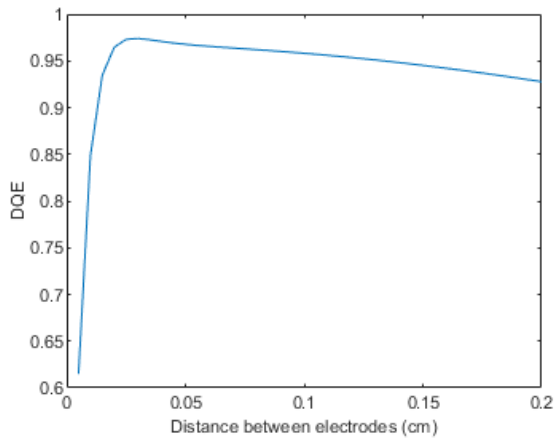

(c)

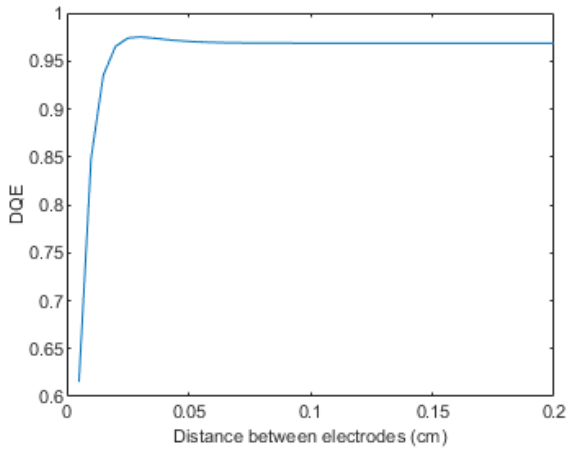

(d)

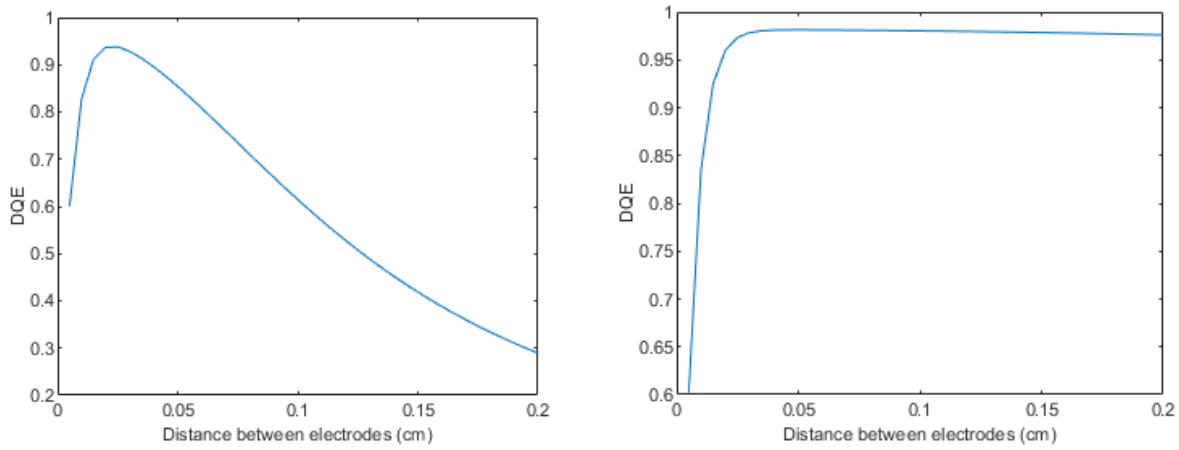

(e) **(f)**

Figure 4.7: Mammography application for conventional poly-$MAPbI_3$ X-ray detector. Detective quantum efficiency (DQE) as a function of photoconductor thickness d. (a) photon energy E=20keV, $\mu\tau= 10^{-5}$ cm^2/V, exposure X=0.6mR, Electrical noise Ne=500e, (b) photon energy E=20keV, $\mu\tau= 10^{-5}$ cm^2/V, exposure X=240mR, Electrical noise Ne=500e, (c) photon energy E=20keV, $\mu\tau= 10^{-6}$ cm^2/V, exposure X=0.6mR, Electrical noise Ne=500e, (d) photon energy E=20keV, $\mu\tau= 10^{-6}$ cm^2/V, exposure X=240mR, Electrical noise Ne=500e, (e) photon energy E=20keV, $\mu\tau= 10^{-7}$ cm^2/V, exposure X=0.6mR, Electrical noise Ne=500e, (f) photon energy E=20keV, $\mu\tau= 10^{-7}$ cm^2/V, exposure X=240mR, Electrical noise Ne=500e.

Figure 4.7 shows the affect of change in electrode distance *d* on DQE for mammography application in conventional structure. In conventional structure, distance between electrodes is considered as photoconductor thickness. The applied electric field was F=1 V/µm and incident photon energy was E=20keV. The nominal exposure of X=0.6mR was used in figure 4.7a, 4.7c, 4.7e, and X=240mR was used for figure 4.7b, 4.7d, 4.7f. The electron hole pair (EHP) creation energy $W_{\pm}$ was 5eV [29]. Electronic noise was 500e. The multiplication of carrier mobility and lifetime was considered same for both electron and hole, which was $\mu\tau= 10^{-5}$ cm^2/V in figure 4.7a and 4.7b, $\mu\tau= 10^{-6}$ cm^2/V in figure 4.7c and 4.7d, and $\mu\tau= 10^{-7}$ cm^2/V in figure 4.7e and 4.7f, respectively.

In figure 4.7a, 4.7b, and 4.7f, DQE gradually increases with the increase of photoconductor thickness and reaches up to 0.99 in figure 4.7a and 4.7b, 0.97 in figure 4.7f. In figure 4.7c and 4.7d, the DQE increases with the photoconductor thickness gradually, and after reaching a peak value at a certain thickness (0.97 at 0.025cm and 0.98 at 0.025cm for figure 4.7c and 4.7d,

respectively), DQE starts to drop slowly if thickness is increased further. In figure 4.7e, DQE reaches the peak value (0.94) for thickness of 0.018cm, then it drops rapidly with increase of thickness.

When noise=1000e and Photon energy=20keV

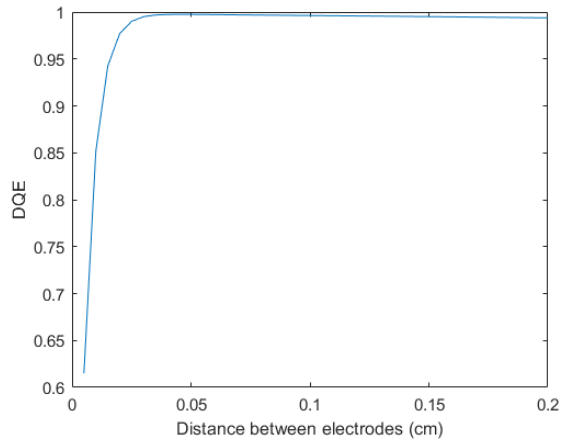

(a)

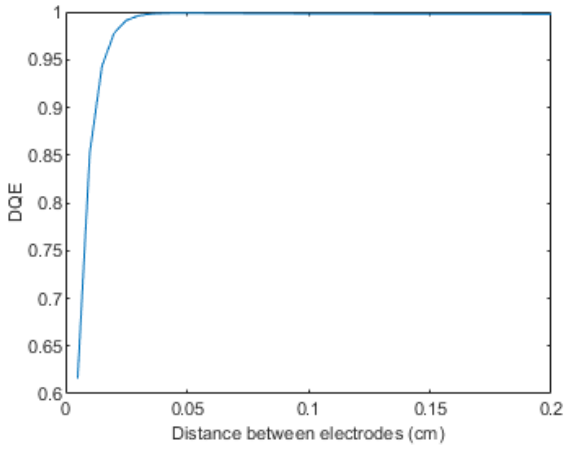

(b)

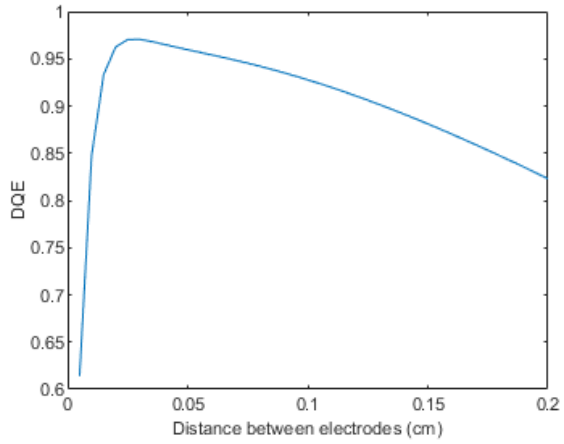

(c)

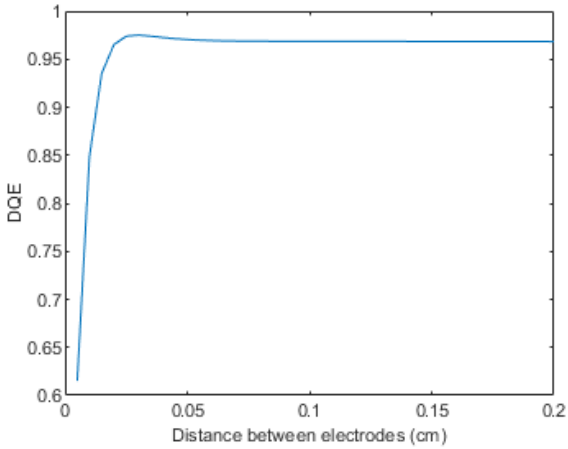

(d)

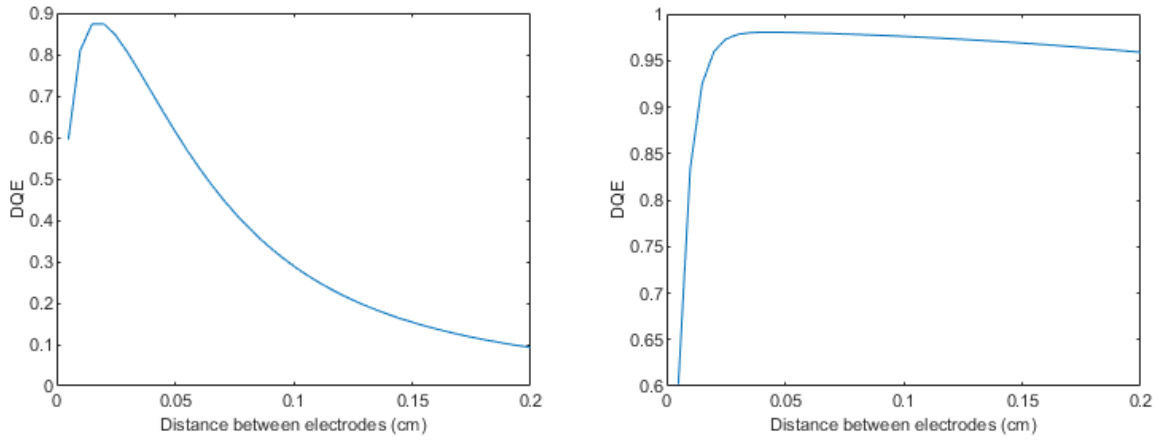

(e) **(f)**

Figure 4.8: Mammography application for conventional poly-$MAPbI_3$ X-ray detector. Detective quantum efficiency (DQE) as a function of photoconductor thickness d. (a) photon energy E=20keV, $\mu\tau= 10^{-5}$ cm^2/V, exposure X=0.6mR, Electrical noise Ne=1000e, (b) photon energy E=20keV, $\mu\tau= 10^{-5}$ cm^2/V, exposure X=240mR, Electrical noise Ne=1000e, (c) photon energy E=20keV, $\mu\tau= 10^{-6}$ cm^2/V, exposure X=0.6mR, Electrical noise Ne=1000e, (d) photon energy E=20keV, $\mu\tau= 10^{-6}$ cm^2/V, exposure X=240mR, Electrical noise Ne=1000e, (e) photon energy E=20keV, $\mu\tau= 10^{-7}$ cm^2/V, exposure X=0.6mR, Electrical noise Ne=1000e, (f) photon energy E=20keV, $\mu\tau= 10^{-7}$ cm^2/V, exposure X=240mR, Electrical noise Ne=1000e.

Figure 4.8 shows the affect of change in electrode distance *d* on DQE for mammography application in conventional structure. In conventional structure, distance between electrodes is considered as photoconductor thickness. The applied electric field was F=1 V/µm and incident photon energy was E=20keV. The nominal exposure of X=0.6mR was used in figure 4.8a, 4.8c, 4.8e, and X=240mR was used for figure 4.8b, 4.8d, 4.8f. The electron hole pair (EHP) creation energy $W_{\pm}$ was 5eV [29]. Electronic noise was 1000e. The multiplication of carrier mobility and lifetime was considered same for both electron and hole, which was $\mu\tau= 10^{-5}$ cm^2/V in figure 4.8a and 4.8b, $\mu\tau= 10^{-6}$ cm^2/V in figure 4.8c and 4.8d, and $\mu\tau= 10^{-7}$ cm^2/V in figure 4.8e and 4.8f, respectively.

In figure 4.8a, and 4.8b, DQE gradually increases with the increase of photoconductor thickness and reaches up to 0.98 in figure 4.8a and 4.8b. In figure 4.8c, 4.8d, and 4.8f, the DQE increases with the photoconductor thickness gradually, and after reaching a peak value at a certain thickness (0.96 at 0.025cm, 0.97 at 0.025cm, and 0.98 at 0.03cm for figure 4.8c, 4.8d and 4.8f,

respectively), DQE starts to drop slowly if thickness is increased further. In figure 4.8e, DQE reaches the peak value (0.85) for thickness of 0.018cm, then it drops rapidly with increase of thickness.

4.2.5: Summary of graphs for poly-$MAPbI_3$

In table 4.1, I have gathered information about the optimum photoconductor thickness l^* and distance between electrodes d^* in different conditions in folded structure for fluoroscopy application. For lower flux, when electronic noise is 1000e and $\mu\tau = 10^{-7}$ cm^2/V, when detector thickness is more than 0.1 cm and distance between electrodes is between 0.0025cm and 0.01cm, we get DQE to be more than 0.8, but if the distance between electrodes are more than 0.01cm, then DQE drops below 0.8. Similarly for higher flux, when electronic noise is 2000e and $\mu\tau = 10^{-7}$ cm^2/V, we get DQE to be more than 0.8 for detector thickness more than 0.07 cm and distance between electrodes is between 0.0025cm and 0.05cm.

Folded Structure, Fluoroscopy							
E=60 keV		l^* (cm)	d^* (cm)	DQE for ψ_{Low}	l^* (cm)	d^* (cm)	DQE for ψ_{High}
Electronic Noise 1000e	$\mu\tau = 10^{-5}$ cm^2/V	>0.07	0.025-0.5	>0.8	>0.07	0.025-0.5	>0.8
	$\mu\tau = 10^{-6}$ cm^2/V	>0.07	0.025-0.1	>0.8	>0.07	0.025-0.5	>0.8
	$\mu\tau = 10^{-7}$ cm^2/V	>0.1	0.0025-0.01	>0.8	>0.07	0.025-0.125	>0.8
Electronic Noise 2000e	$\mu\tau = 10^{-5}$ cm^2/V	>0.07	0.025-0.5	>0.8	>0.06	0.025-0.5	>0.8
	$\mu\tau = 10^{-6}$ cm^2/V	>0.08	0.0025-0.045	>0.8	>0.07	0.025-0.5	>0.8
	$\mu\tau = 10^{-7}$ cm^2/V	>0.08	0.0025-0.005	>0.7	>0.07	0.0025-0.05	>0.8

Table 4.1: Design guideline for fluoroscopy application for folded poly-$MAPbI_3$ X-ray detector. For photon energy E=60keV, performance of DQE is measured for low (0.1μR) and high exposure (10μR) along with different electronic noise (1000e and 2000e).

In table 4.2, I have gathered information about the optimum photoconductor thickness l^* and distance between electrodes d^* in different conditions in folded structure for mammography application. For instance, while using lower flux, electronic noise of 1000e, $\mu\tau = 10^{-7}$ cm^2/V, when detector thickness is more than 0.01 cm and distance between electrodes is between

0.0025cm and 0.0325cm, then we get DQE to be more than 0.8, but if the distance between electrodes are more than 0.0325cm, then DQE drops below 0.8.

Folded Structure, Mammography							
E=20 keV		l^* (cm)	d^* (cm)	DQE for ψ_{Low}	l^* (cm)	d^* (cm)	DQE for ψ_{High}
Electrical Noise 500e	$\mu\tau$ =10^{-5} cm^2/V	>0.01	0.025-0.5	>0.8	>0.01	0.025-0.5	>0.8
	$\mu\tau$ =10^{-6} cm^2/V	>0.01	0.025-0.5	>0.8	>0.01	0.025-0.5	>0.8
	$\mu\tau$ =10^{-7} cm^2/V	>0.01	0.0025-0.05	>0.8	>0.01	0.025-0.05	>0.8
Electrical Noise 1000e	$\mu\tau$ =10^{-5} cm^2/V	>0.01	0.025-0.5	>0.8	>0.01	0.025-0.5	>0.8
	$\mu\tau$ =10^{-6} cm^2/V	>0.01	0.025-0.325	>0.8	>0.01	0.025-0.5	>0.8
	$\mu\tau$ =10^{-7} cm^2/V	>0.01	0.0025-0.0325	>0.8	>0.01	0.025-0.5	>0.8

Table 4.2: Design guideline for mammography application for folded poly-$MAPbI_3$ X-ray detector. For photon energy E=20keV, performance of DQE is measured for low (0.6mR) and high exposure (240mR) along with different electronic noise (500e and 1000e).

In table 4.3, we have gathered information about the optimum distance between electrodes *d** in different conditions in conventional structure for fluoroscopy application. For instance, while using lower flux, electronic noise of 1000e, $\mu\tau$ =10^{-7} cm^2/V, when distance between electrodes is between 0.006cm and 0.06cm, we get DQE to be more than 0.1, but if the distance between electrodes are more than 0.06cm, then DQE drops below 0.1. Again, for higher flux (higher exposure), electronic noise of 1000e, $\mu\tau$ =10^{-6} cm^2/V, if distance between electrodes is more than 0.065 cm, we get DQE to be more than 0.8. But if distance between electrodes is more than 0.065cm, than DQE drops below 0.8.

Conventional Structure, Fluoroscopy					
E=60 keV		d^* (cm)	DQE for ψ_{Low}	d^* (cm)	DQE for ψ_{High}
Electrical Noise	$\mu\tau$ =10^{-5} cm^2/V	>0.06	>0.8	>0.06	>0.8
	$\mu\tau$ =10^{-6} cm^2/V	0.055-0.14	>0.7	>0.065	>0.8

1000e	$\mu\tau$ =10^{-7} cm^2/V	0.006-0.06	>0.1	0.085-0.1	>0.8
Electrical Noise 2000e	$\mu\tau$ =10^{-5} cm^2/V	>0.065	>0.8	>0.06	>0.8
	$\mu\tau$ =10^{-6} cm^2/V	0.035-0.1	>0.5	>0.065	>0.8
	$\mu\tau$ =10^{-7} cm^2/V	0.005-0.035	>0.05	0.045-0.085	>0.6

Table 4.3: Design guideline for fluoroscopy application for conventional poly-$MAPbI_3$ X-ray detector. For photon energy E=60keV, performance of DQE is measured for low (0.1μR) and high exposure (10μR) along with different electronic noise (1000e and 2000e).

In table 4.4, we have gathered information about the optimum distance between electrodes d^* in different conditions in conventional structure for mammography application. For instance, while using lower flux, electronic noise of 500e, $\mu\tau$ =10^{-7} cm^2/V, when distance between electrodes is between 0.008cm to 0.06cm, we get DQE to be more than 0.8, but if the distance between electrodes are more than 0.06cm, then DQE drops below 0.8. Again, for higher flux (higher exposure), electronic noise of 1000e, $\mu\tau$ =10^{-6} cm^2/V, if distance between electrodes is more than 0.008cm, we get DQE to be more than 0.8. But if distance between electrodes is more than 0.008cm, than DQE drops below 0.8.

Conventional Structure, Mammography					
E=20 keV		d^* (cm)	DQE for ψ_{Low}	d^* (cm)	DQE for ψ_{High}
Electrical Noise 500e	$\mu\tau$ =10^{-5} cm^2/V	>0.009	>0.8	>0.008	>0.8
	$\mu\tau$ =10^{-6} cm^2/V	>0.009	>0.8	>0.008	>0.8
	$\mu\tau$ =10^{-7} cm^2/V	>0.008-0.06	>0.8	>0.008	>0.8
Electrical Noise 1000e	$\mu\tau$ =10^{-5} cm^2/V	>0.008	>0.8	>0.08	>0.8
	$\mu\tau$ =10^{-6} cm^2/V	>0.008	>0.8	>0.008	>0.8
	$\mu\tau$ =10^{-7} cm^2/V	0.01-0.03	>0.8	>0.009	>0.8

Table 4.4. Design guideline for mammography application for conventional poly-$MAPbI_3$ X-ray detector. For photon energy E=20keV, performance of DQE is measured for low (0.6mR) and high exposure (240mR) along with different electronic noise (500e and 1000e).

From the above discussion, we can say for folded structure provides much better DQE than conventional structure for fluoroscopy application. But for mammography application, both folded and conventional structure provides good DQE (more than 0.8) with almost identical

performance, but folded structure is slightly ahead because it provides same DQE in relatively less photoconductor thickness.

4.3: Amorphous Selenium

The DQE performance of amorphous selenium detector having folded, and conventional structures was evaluated for both fluoroscopy and mammography applications. The thickness of the electrode in the folded structure is assumed to be d_{foil}=2.8μm [**Error! Bookmark not defined.**]. The electric field is considered to be F = 10 V/μm. The average photon energies are assumed to be 60 keV and 20 keV for fluoroscopy and mammographic applications, respectively. The hole mobility μ_h=0.12 $cm^2V^{-1}s^{-1}$, electron mobility μ_e=0.003 $cm^2V^{-1}s^{-1}$, hole lifetime τ_h=50 μs, electron lifetime τ_e=200 μs. While calculating detective quantum efficiency, different ranges of exposure are used for different applications. The range of exposure varies from 0.1 to 10 μR with the mean exposure being 1 μR in Fluoroscopy application where it varies from 0.6 to 240 mR with the mean exposure being 12 mR in mammography application. Several sources of electronic noise are associated with the read-out technology. TFT reset noise or kTC noise (typical value is 600 *e*) is the dominant source of electronic noise, data line and charge amplifier noise (typical value is 800–2000 *e* in passive pixel) per pixel also plays a big role. The total noise power is the sum of the noise power of all the sources, and each of the component sources of noise is independent. The pixel size for fluoroscopic image sensors is large and the total electronic noise (N_e) typically varies from 1000 e to 2000 e per pixel whereas it varies from 500 *e* to 1000 *e* per pixel in mammographic detectors due to their smaller pixel size and the use of CMOS or active pixel technology [23]. The noise power, $S_{Ne} = N_e^2$.

4.3.1: Folded Structure (Fluoroscopy)

The effect of electric field, exposure, carrier density, electronic noise on DQE were studied for fluoroscopy. For fluoroscopy application, pixel area is 200 μm × 200 μm.

When noise=1000e and Photon energy=60keV (Positive bias)

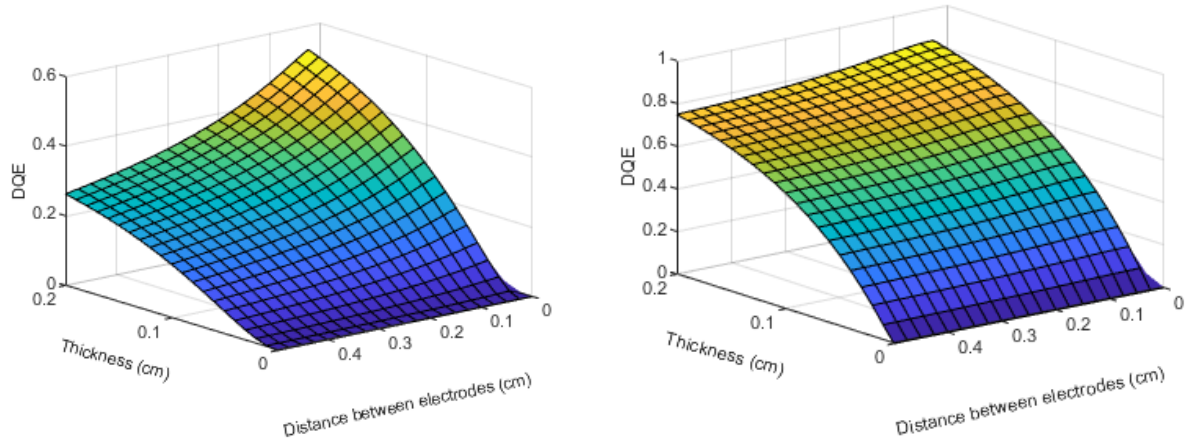

(a) **(b)**

Figure 4.9: Fluoroscopy application for folded amorphous Se X-ray detector. Detective quantum efficiency (DQE) as a function of photoconductor thickness *l* and distance between electrodes *d*. (a) photon energy E=60keV, hole mobility μ_h=0.12 $cm^2V^{-1}s^{-1}$, electron mobility μ_e=0.003 $cm^2V^{-1}s^{-1}$, hole lifetime τ_h=50 µs, electron lifetime τ_e=200 µs, exposure X=0.1µR, Electrical noise Ne=1000e, (b) photon energy E=60keV, hole mobility μ_h=0.12 $cm^2V^{-1}s^{-1}$, electron mobility μ_e=0.003 $cm^2V^{-1}s^{-1}$, hole lifetime τ_h=50 µs, electron lifetime τ_e=200 µs, exposure X=10µR, Electrical noise Ne=1000e.

Figure 4.9 shows the effect of change in photoconductor thickness *l* and electrode distance *d* on DQE for fluoroscopy application in folded structure. The applied electric field was F=10 V/µm and incident photon energy was E=60keV. The nominal exposure of X=0.1µR was used in figure 4.9a, and X=10µR was used for figure 4.9b. The electron hole pair (EHP) creation energy $W_{\pm}$ was 45eV [29]. Electronic noise was 1000e. Hole mobility μ_h=0.12 $cm^2V^{-1}s^{-1}$, electron mobility μ_e=0.003 $cm^2V^{-1}s^{-1}$, hole lifetime τ_h=50 µs, and electron lifetime τ_e=200 µs.

In figure 4.9a, at first DQE increases almost linearly with the increase of photoconductor thickness. Then the DQE increases slowly with increase in thickness. At the same time, at first DQE increases rapidly with the increase of distance between charging electrodes. After reaching the pick value at a certain *d* (0.55 at 0.03cm), DQE starts to decrease with the increase of distance between electrodes.

In figure 4.9b, the DQE increases with the increase of photoconductor thickness gradually. At the same time, at first DQE increases with the increase in distance between electrodes, and after

reaching a certain value of *d* (0.03cm), DQE reaches the maximum value (0.85), then starts to decrease if distance between electrodes is increased.

When noise=2000e and Photon energy=60keV (Positive bias)

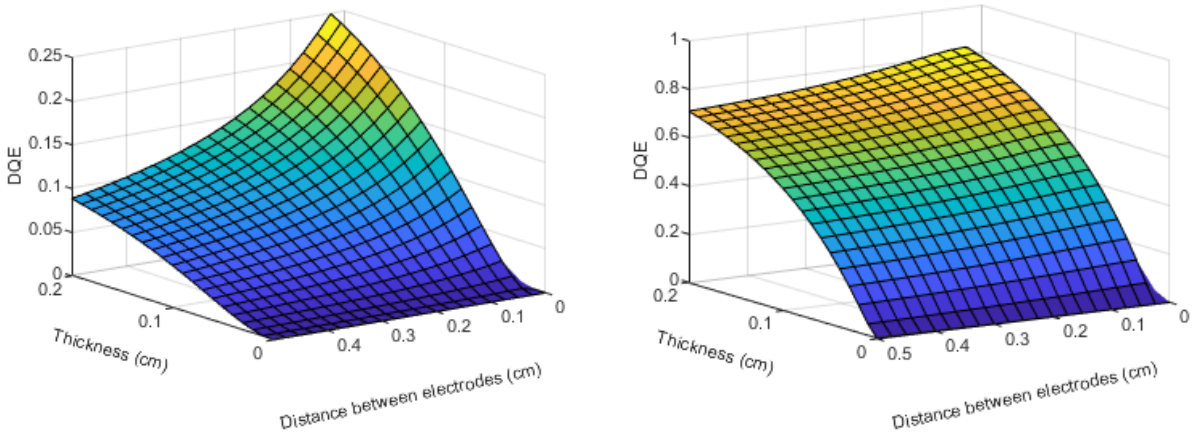

(a) **(b)**

Figure 4.10: Fluoroscopy application for folded amorphous Se X-ray detector. Detective quantum efficiency (DQE) as a function of photoconductor thickness *l* and distance between electrodes *d*. (a) photon energy E=60keV, hole mobility μ_h=0.12 $cm^2V^{-1}s^{-1}$, electron mobility μ_e=0.003 $cm^2V^{-1}s^{-1}$, hole lifetime τ_h=50 µs, electron lifetime τ_e=200 µs, exposure X=0.1µR, Electrical noise Ne=2000e, (b) photon energy E=60keV, hole mobility μ_h=0.12 $cm^2V^{-1}s^{-1}$, electron mobility μ_e=0.003 $cm^2V^{-1}s^{-1}$, hole lifetime τ_h=50 µs, electron lifetime τ_e=200 µs, exposure X=10µR, Electrical noise Ne=2000e.

Figure 4.10 shows the affect of change in photoconductor thickness *l* and electrode distance *d* on DQE for fluoroscopy application in folded structure. The applied electric field was F=10 V/µm and incident photon energy was E=60keV. The nominal exposure of X=0.1µR was used in figure 4.10a, and X=10µR was used for figure 4.10b. The electron hole pair (EHP) creation energy $W_{\pm}$ was 45eV [29]. Electronic noise was 2000e. Hole mobility μ_h=0.12 $cm^2V^{-1}s^{-1}$, electron mobility μ_e=0.003 $cm^2V^{-1}s^{-1}$, hole lifetime τ_h=50 µs, and electron lifetime τ_e=200 µs.

In figure 4.10a, at first DQE increases almost linearly with the increase of photoconductor. Then the DQE increases slowly with increase in thickness. At the same time, at first DQE increases rapidly with the increase of distance between charging electrodes. After reaching the pick value

at a certain *d* (0.25 at 0.03cm), DQE starts to decrease with the increase of distance between electrodes.

In figure 4.10b, the DQE increases with the increase of photoconductor thickness gradually. At the same time, at first DQE increases with the increase in distance between electrodes, and after reaching a certain value of *d* (0.03cm), DQE reaches the maximum value (0.83), then starts to decrease if distance between electrodes is increased.

4.3.2: Folded Structure (Mammography)

The effect of electric field, exposure, carrier density, electronic noise on DQE were studied for mammography. For mammography application, pixel area is 50 μm × 50 μm.

When noise=500e and Photon energy=20keV (Positive bias)

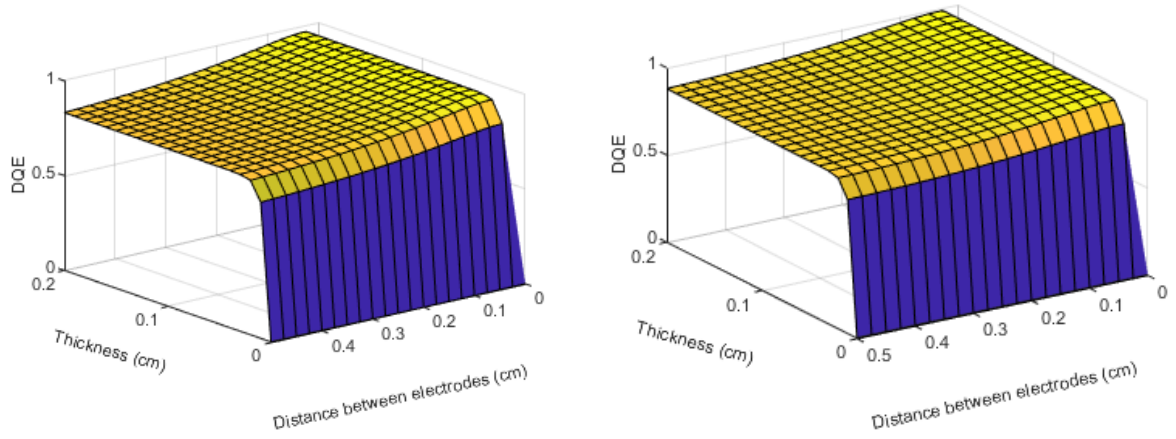

(a) **(b)**

Figure 4.11: Mammography application for folded amorphous Se X-ray detector. Detective quantum efficiency (DQE) as a function of photoconductor thickness *l* and distance between electrodes *d*. (a) photon energy E=20keV, hole mobility μ_h=0.12 $cm^2V^{-1}s^{-1}$, electron mobility μ_e=0.003 $cm^2V^{-1}s^{-1}$, hole lifetime τ_h=50 μs, electron lifetime τ_e=200 μs, exposure X= 0.6 mR, Electrical noise Ne=500e, (b) photon energy E=20keV, hole mobility μ_h=0.12 $cm^2V^{-1}s^{-1}$, electron mobility μ_e=0.003 $cm^2V^{-1}s^{-1}$, hole lifetime τ_h=50 μs, electron lifetime τ_e=200 μs, exposure X=240 mR, Electrical noise Ne=500e.

Figure 4.11 shows the affect of change in photoconductor thickness *l* and electrode distance *d* on DQE for mammography application in folded structure. The applied electric field was F=10 V/μm and incident photon energy was E=20keV. The nominal exposure of X=0.6 mR was used in figure 4.11a, and X=240 mR was used for figure 4.11b. The electron hole pair (EHP) creation energy $W_{\pm}$ was 45eV [29]. Electronic noise was 500e. Hole mobility μ_h=0.12 $cm^2V^{-1}s^{-1}$, electron mobility μ_e=0.003 $cm^2V^{-1}s^{-1}$, hole lifetime τ_h=50 μs, and electron lifetime τ_e=200 μs.

In figure 4.11a, at first DQE increases almost linearly with the increase of photoconductor. Then the DQE increases slowly with increase of photoconductor thickness (from 0.03cm). At the same time, at first DQE increases rapidly with the increase of distance between charging electrodes. After reaching the pick value at a certain *d* (0.92 at 0.025cm), DQE starts to decrease with the increase of distance between electrodes.

In figure 4.11b, the DQE increases with the increase of photoconductor thickness gradually. At the same time, at first DQE increases with the increase in distance between electrodes, and after reaching a certain value of *d*, DQE starts to decrease, then again start to rise, and will decrease after reaching a certain value of *d*. Although DQE is showing increasing trend with *d* in our measurement range, after a certain value of *d* (0.025cm), DQE should reach its maximum value (0.97) and start to decrease with the increase of distance between electrodes.

When noise=1000e and Photon energy=20keV (Positive bias)

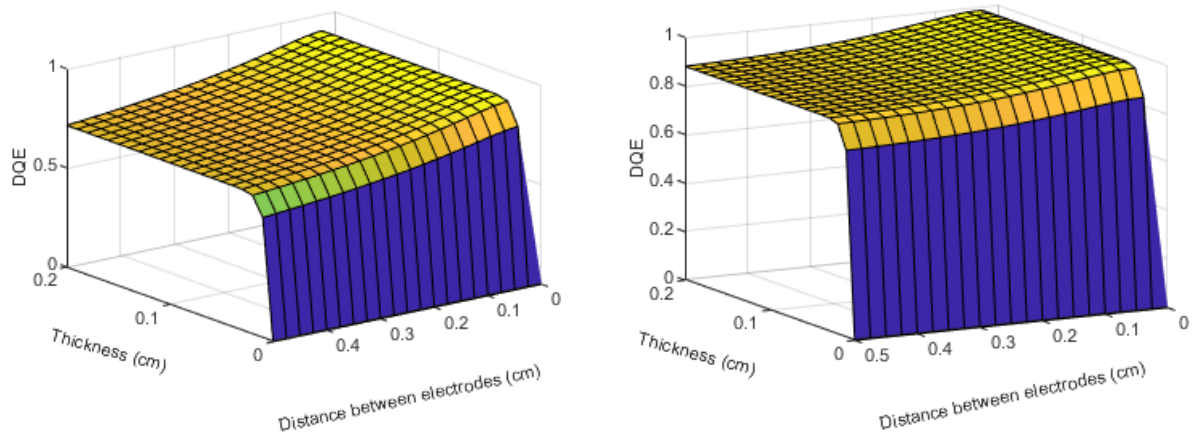

(a) **(b)**

Figure 4.12: Mammography application for folded amorphous Se X-ray detector. Detective quantum efficiency (DQE) as a function of photoconductor thickness l and distance between electrodes d. (a) photon energy E=20keV, hole mobility μ_h=0.12 $cm^2V^{-1}s^{-1}$, electron mobility μ_e=0.003 $cm^2V^{-1}s^{-1}$, hole lifetime τ_h=50 μs, electron lifetime τ_e=200 μs, exposure X= 0.6 mR, Electrical noise Ne=1000e, (b) photon energy E=20keV, hole mobility μ_h=0.12 $cm^2V^{-1}s^{-1}$, electron mobility μ_e=0.003 $cm^2V^{-1}s^{-1}$, hole lifetime τ_h=50 μs, electron lifetime τ_e=200 μs, exposure X=240 mR, Electrical noise Ne=1000e.

Figure 4.12 shows the affect of change in photoconductor thickness l and electrode distance d on DQE for mammography application in folded structure. The applied electric field was F=10 V/μm and incident photon energy was E=20keV. The nominal exposure of X=0.6 mR was used in figure 4.12a, and X=240 mR was used for figure 4.12b. The electron hole pair (EHP) creation energy $W_{\pm}$ was 45eV [29]. Electronic noise was 1000e. Hole mobility μ_h=0.12 $cm^2V^{-1}s^{-1}$, electron mobility μ_e=0.003 $cm^2V^{-1}s^{-1}$, hole lifetime τ_h=50 μs, and electron lifetime τ_e=200 μs.

In figure 4.12a, at first DQE increases almost linearly with the increase of photoconductor. Then the DQE increases slowly with increase of photoconductor thickness (from 0.03cm). At the same time, at first DQE increases rapidly with the increase of distance between charging electrodes. After reaching the pick value at a certain d (0.8 at 0.025cm), DQE starts to decrease with the increase of distance between electrodes.

In figure 4.12b, the DQE increases with the increase of photoconductor thickness gradually. At the same time, at first DQE increases with the increase in distance between electrodes, and after reaching a certain value of d, DQE starts to decrease, then again start to rise, and will decrease after reaching a certain value of d. Although DQE is showing increasing trend with d in our measurement range, after a certain value of d (0.025cm), DQE should reach its maximum value (0.93) and start to decrease with the increase of distance between electrodes.

4.3.3: Conventional Structure (Fluoroscopy, Positive Bias)

The effect of electric field, exposure, carrier density, electronic noise on DQE were studied for fluoroscopy. For fluoroscopy application, pixel area is 200 μm × 200 μm. This study was conducted for positive bias to the photodetector.

When noise=1000e and Photon energy=60keV (Positive bias)

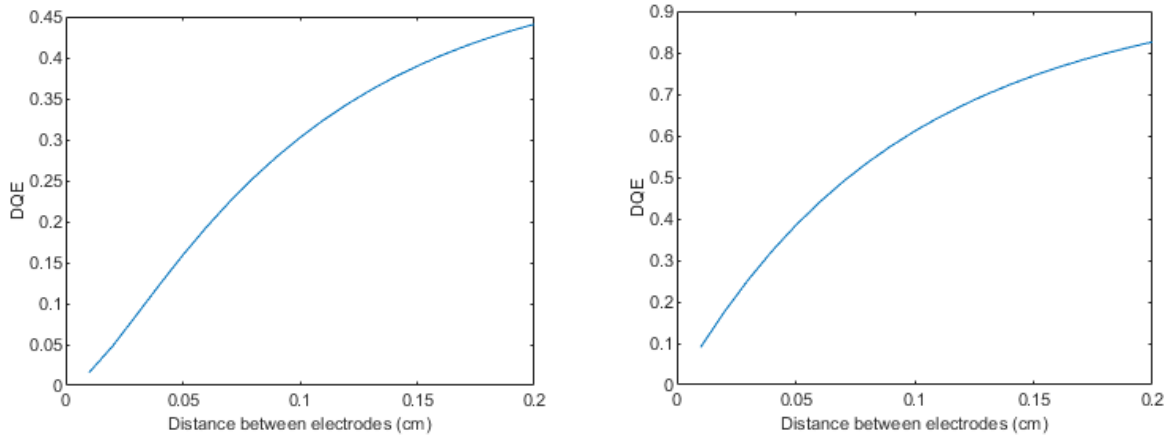

(a) **(b)**

Figure 4.13: Fluoroscopy application for folded amorphous Se X-ray detector. Detective quantum efficiency (DQE) as a function of photoconductor thickness d. (a) photon energy E=60keV, hole mobility μ_h=0.12 $cm^2V^{-1}s^{-1}$, electron mobility μ_e=0.003 $cm^2V^{-1}s^{-1}$, hole lifetime τ_h=50 µs, electron lifetime τ_e=200 µs, exposure X= 0.1 µR, Electrical noise Ne=1000e, (b) photon energy E=60keV, hole mobility μ_h=0.12 $cm^2V^{-1}s^{-1}$, electron mobility μ_e=0.003 $cm^2V^{-1}s^{-1}$, hole lifetime τ_h=50 µs, electron lifetime τ_e=200 µs, exposure X= 10 µR, Electrical noise Ne=1000e.

Figure 4.13 shows the affect of change in electrode distance *d* on DQE for fluoroscopy application in conventional structure. In conventional structure, distance between electrodes is considered as photoconductor thickness. The applied electric field was F=10 V/µm and incident photon energy was E=60keV. The nominal exposure of X=0.1µR was used in figure 4.13a, and X=10µR was used for figure 4.13b. The electron hole pair (EHP) creation energy $W_{\pm}$ was 45eV [29]. Electronic noise was 1000e. Hole mobility μ_h=0.12 $cm^2V^{-1}s^{-1}$, electron mobility μ_e=0.003 $cm^2V^{-1}s^{-1}$, hole lifetime τ_h=50 µs, and electron lifetime τ_e=200 µs.

In figure 4.13a and 4.13b, DQE gradually increases with the increase of photoconductor thickness. But imaging performance is poor in this combination. The maximum DQE are 0.44 and 0.83 for figure 4.13a and 4.13b, respectively.

When noise=2000e and Photon energy=60keV (Positive bias)

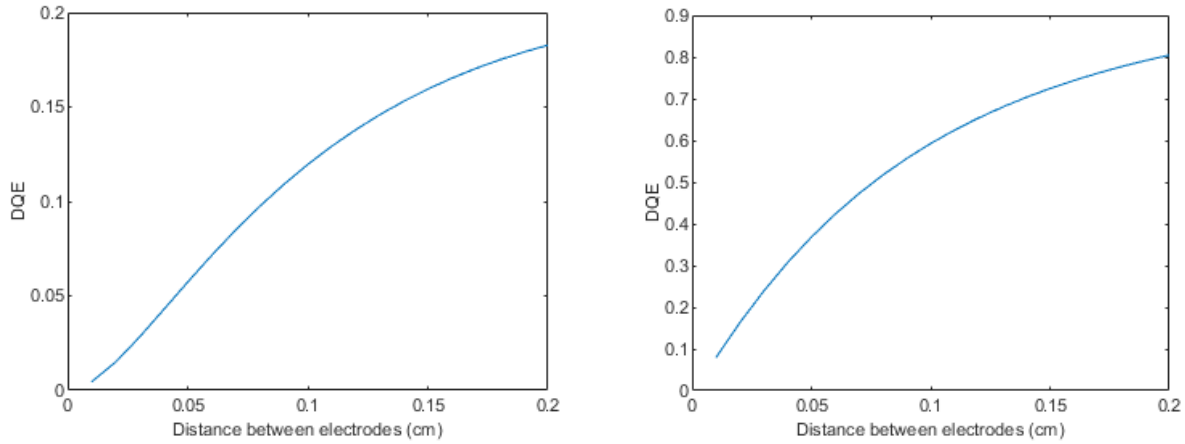

(a) **(b)**

Figure 4.14: Fluoroscopy application for folded amorphous Se X-ray detector. Detective quantum efficiency (DQE) as a function of photoconductor thickness d. (a) photon energy E=60keV, hole mobility μ_h=0.12 $cm^2V^{-1}s^{-1}$, electron mobility μ_e=0.003 $cm^2V^{-1}s^{-1}$, hole lifetime τ_h=50 µs, electron lifetime τ_e=200 µs, exposure X= 0.1 µR, Electrical noise Ne=2000e, (b) photon energy E=60keV, hole mobility μ_h=0.12 $cm^2V^{-1}s^{-1}$, electron mobility μ_e=0.003 $cm^2V^{-1}s^{-1}$, hole lifetime τ_h=50 µs, electron lifetime τ_e=200 µs, exposure X= 10 µR, Electrical noise Ne=2000e.

Figure 4.14 shows the affect of change in electrode distance *d* on DQE for fluoroscopy application in conventional structure. In conventional structure, distance between electrodes is considered as photoconductor thickness. The applied electric field was F=10 V/µm and incident photon energy was E=60keV. The nominal exposure of X=0.1µR was used in figure 4.14a, and X=10µR was used for figure 4.14b. The electron hole pair (EHP) creation energy $W_{\pm}$ was 45eV [29]. Electronic noise was 2000e. Hole mobility μ_h=0.12 $cm^2V^{-1}s^{-1}$, electron mobility μ_e=0.003 $cm^2V^{-1}s^{-1}$, hole lifetime τ_h=50 µs, and electron lifetime τ_e=200 µs.

In figure 4.14a and 4.14b, DQE gradually increases with the increase of photoconductor thickness. But imaging performance is poor in this combination. The maximum DQE are 0.18 and 0.81 for figure 4.14a and 4.14b, respectively.

4.3.4: Conventional Structure (Mammography, Positive Bias)

Findings for mammography in folded structure is presented here. For mammography application, pixel area is 50 µm × 50 µm. This study was conducted for positive bias to the photodetector.

When noise=500e and Photon energy=20keV (Positive bias)

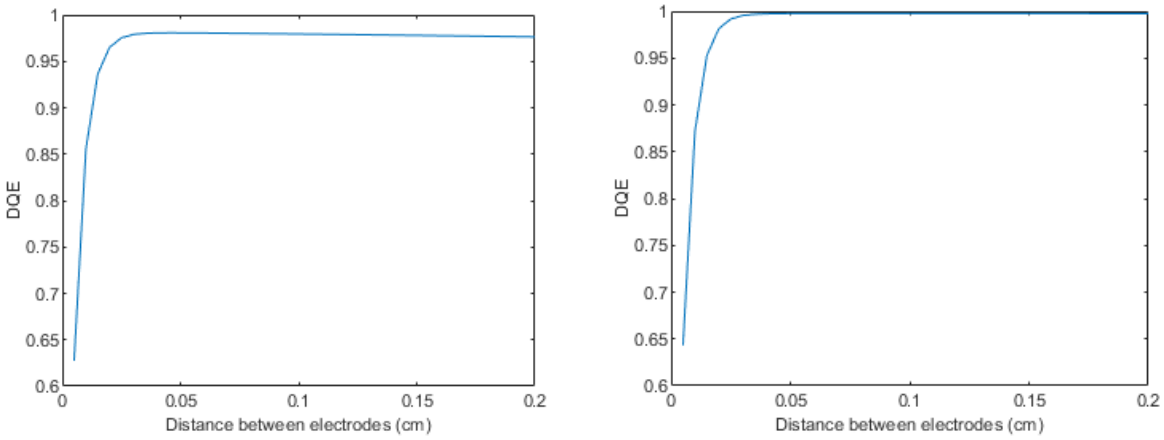

(a) **(b)**

Figure 4.15: Mammography application for folded amorphous Se X-ray detector. Detective quantum efficiency (DQE) as a function of photoconductor thickness d. (a) photon energy E=20keV, hole mobility μ_h=0.12 $cm^2V^{-1}s^{-1}$, electron mobility μ_e=0.003 $cm^2V^{-1}s^{-1}$, hole lifetime τ_h=50 µs, electron lifetime τ_e=200 µs, exposure X= 0.6 mR, Electrical noise Ne=500e, (b) photon energy E=20keV, hole mobility μ_h=0.12 $cm^2V^{-1}s^{-1}$, electron mobility μ_e=0.003 $cm^2V^{-1}s^{-1}$, hole lifetime τ_h=50 µs, electron lifetime τ_e=200 µs, exposure X= 240 mR, Electrical noise Ne=500e.

Figure 4.15 shows the affect of change in electrode distance *d* on DQE for mammography application in conventional structure. In conventional structure, distance between electrodes is considered as photoconductor thickness. The applied electric field was F=10 V/µm and incident photon energy was E=20keV. The nominal exposure of X=0.6 mR was used in figure 4.15a, and X=240 mR was used for figure 4.15b. The electron hole pair (EHP) creation energy $W_{\pm}$ was 45eV [29]. Electronic noise was 500e. Hole mobility μ_h=0.12 $cm^2V^{-1}s^{-1}$, electron mobility μ_e=0.003 $cm^2V^{-1}s^{-1}$, hole lifetime τ_h=50 µs, and electron lifetime τ_e=200 µs.

In figure 4.15a, the DQE increases with the photoconductor thickness gradually, and after the DQE reaches the peak value at a certain distance between charge collecting electrodes (0.97 at 0.03cm), DQE starts to drop slowly if thickness is increased further. In figure 4.15b, DQE

gradually increases with the increase of photoconductor thickness. Maximum DQE of about 0.99 is observed at 0.1cm of photoconductor thickness.

When noise=1000e and Photon energy=20keV (Positive bias)

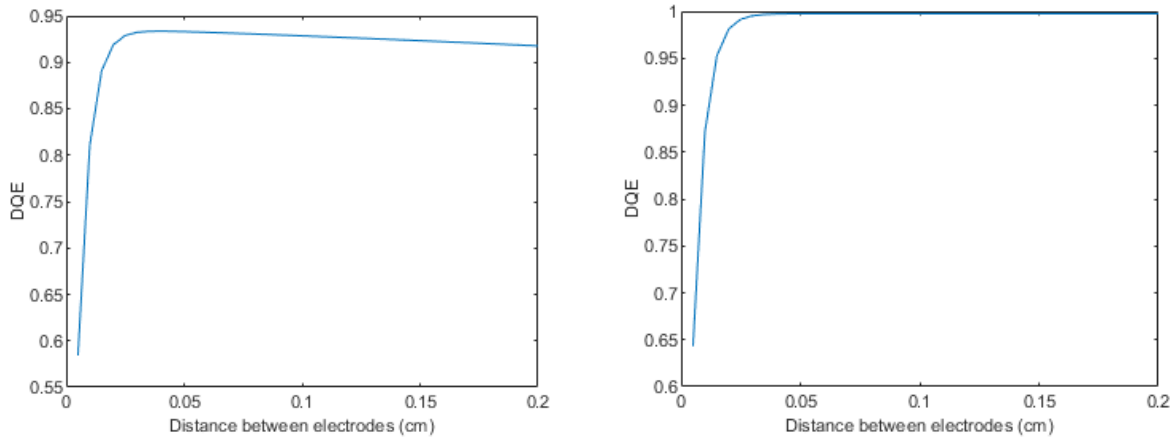

(a) **(b)**

Figure 4.16: Mammography application for folded amorphous Se X-ray detector. Detective quantum efficiency (DQE) as a function of photoconductor thickness d. (a) photon energy E=20keV, hole mobility μ_h=0.12 $cm^2V^{-1}s^{-1}$, electron mobility μ_e=0.003 $cm^2V^{-1}s^{-1}$, hole lifetime τ_h=50 µs, electron lifetime τ_e=200 µs, exposure X= 0.6 mR, Electrical noise Ne=1000e, (b) photon energy E=20keV, hole mobility μ_h=0.12 $cm^2V^{-1}s^{-1}$, electron mobility μ_e=0.003 $cm^2V^{-1}s^{-1}$, hole lifetime τ_h=50 µs, electron lifetime τ_e=200 µs, exposure X= 240 mR, Electrical noise Ne=1000e.

Figure 4.16 shows the affect of change in electrode distance *d* on DQE for mammography application in conventional structure. In conventional structure, distance between electrodes is considered as photoconductor thickness. The applied electric field was F=10 V/µm and incident photon energy was E=20keV. The nominal exposure of X=0.6 mR was used in figure 4.16a, and X=240 mR was used for figure 4.16b. The electron hole pair (EHP) creation energy $W_{\pm}$ was 45eV [29]. Electronic noise was 1000e. Hole mobility μ_h=0.12 $cm^2V^{-1}s^{-1}$, electron mobility μ_e=0.003 $cm^2V^{-1}s^{-1}$, hole lifetime τ_h=50 µs, and electron lifetime τ_e=200 µs.

In figure 4.16a, the DQE increases with the photoconductor thickness gradually, and after the DQE reaches the peak value at a certain distance between charge collecting electrodes (0.93 at

0.025cm), DQE starts to drop slowly if thickness is increased further. In figure 4.16b, DQE gradually increases with the increase of photoconductor thickness. Maximum DQE of about 0.99 is observed at 0.1cm of photoconductor thickness.

4.3.5: Conventional Structure (Fluoroscopy, Negative Bias)

Findings for fluoroscopy in folded structure is presented here. For fluoroscopy application, pixel area is 200 µm × 200 µm. This study was conducted for negative bias to the photodetector.

When noise=1000e and Photon energy=60keV (Negative bias)

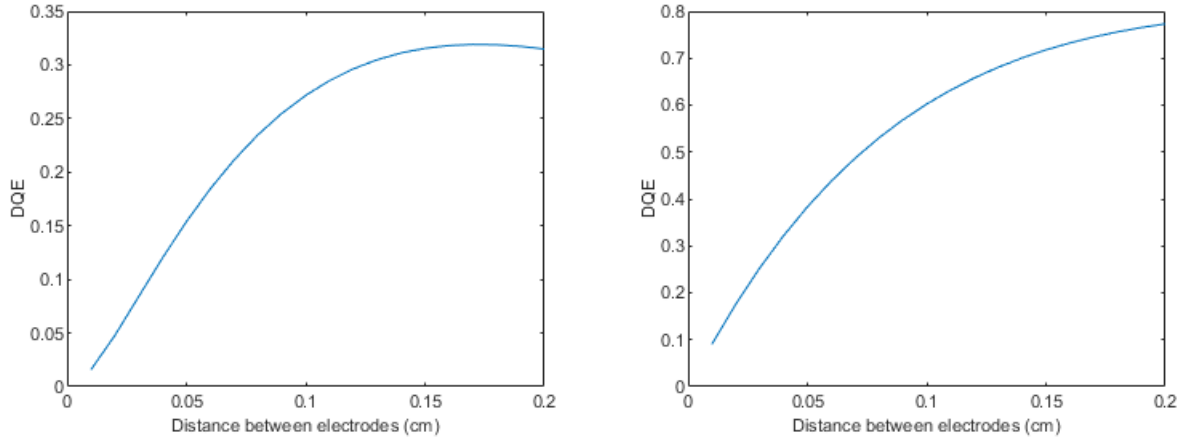

(a) **(b)**

Figure 4.17: Mammography application for folded amorphous Se X-ray detector. Detective quantum efficiency (DQE) as a function of photoconductor thickness d. (a) photon energy E=20keV, hole mobility μ_h=0.12 $cm^2V^{-1}s^{-1}$, electron mobility μ_e=0.003 $cm^2V^{-1}s^{-1}$, hole lifetime τ_h=50 µs, electron lifetime τ_e=200 µs, exposure X= 0.6 mR, Electrical noise Ne=1000e, (b) photon energy E=20keV, hole mobility μ_h=0.12 $cm^2V^{-1}s^{-1}$, electron mobility μ_e=0.003 $cm^2V^{-1}s^{-1}$, hole lifetime τ_h=50 µs, electron lifetime τ_e=200 µs, exposure X=240 mR, Electrical noise Ne=1000e.

Figure 4.17 shows the affect of change in electrode distance *d* on DQE for fluoroscopy application in conventional structure. In conventional structure, distance between electrodes is considered as photoconductor thickness. The applied electric field was F=10 V/µm and incident photon energy was E=60keV. The nominal exposure of X=0.1µR was used in figure 4.17a, and X=10µR was used for figure 4.17b. The electron hole pair (EHP) creation energy $W_{\pm}$ was 45eV

[29]. Electronic noise was 1000e. Hole mobility μ_h=0.12 $cm^2V^{-1}s^{-1}$, electron mobility μ_e=0.003 $cm^2V^{-1}s^{-1}$, hole lifetime τ_h=50 µs, and electron lifetime τ_e=200 µs.

In figure 4.17a and 4.17b, DQE gradually increases with the increase of photoconductor thickness. But imaging performance is poor in this combination. The maximum DQE are 0.31 and 0.78 for figure 4.17a and 4.17b, respectively.

When noise=2000e and Photon energy=60keV (Negative bias)

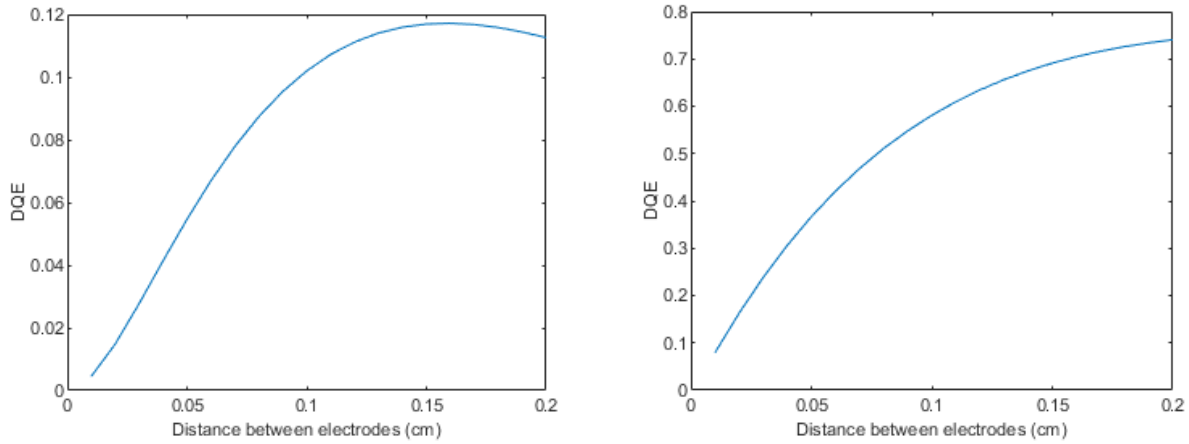

(a) **(b)**

Figure 4.18: Fluoroscopy application for folded amorphous Se X-ray detector. Detective quantum efficiency (DQE) as a function of photoconductor thickness d. (a) photon energy E=60keV, hole mobility μ_h=0.12 $cm^2V^{-1}s^{-1}$, electron mobility μ_e=0.003 $cm^2V^{-1}s^{-1}$, hole lifetime τ_h=50 µs, electron lifetime τ_e=200 µs, exposure X= 0.1 µR, Electrical noise Ne=2000e, (b) photon energy E=60keV, hole mobility μ_h=0.12 $cm^2V^{-1}s^{-1}$, electron mobility μ_e=0.003 $cm^2V^{-1}s^{-1}$, hole lifetime τ_h=50 µs, electron lifetime τ_e=200 µs, exposure X= 10 µR, Electrical noise Ne=2000e.

Figure 4.18 shows the affect of change in electrode distance *d* on DQE for fluoroscopy application in conventional structure. In conventional structure, distance between electrodes is considered as photoconductor thickness. The applied electric field was F=10 V/µm and incident photon energy was E=60keV. The nominal exposure of X=0.1µR was used in figure 4.18a, and X=10µR was used for figure 4.18b. The electron hole pair (EHP) creation energy $W_{\pm}$ was 45eV [29]. Electronic noise was 2000e. Hole mobility μ_h=0.12 $cm^2V^{-1}s^{-1}$, electron mobility μ_e=0.003 $cm^2V^{-1}s^{-1}$, hole lifetime τ_h=50 µs, and electron lifetime τ_e=200 µs.

In figure 4.18a and 4.18b, DQE gradually increases with the increase of photoconductor thickness. But imaging performance is poor in this combination. The maximum DQE are 0.11 and 0.74 for figure 4.18a and 4.18b, respectively.

4.3.6: Conventional Structure (Mammography, Negative Bias)

Findings for mammography in folded structure is presented here. For mammography application, pixel area is 50 μm × 50 μm. This study was conducted for negative bias to the photodetector.

When noise=500e and Photon energy=20keV (Negative bias)

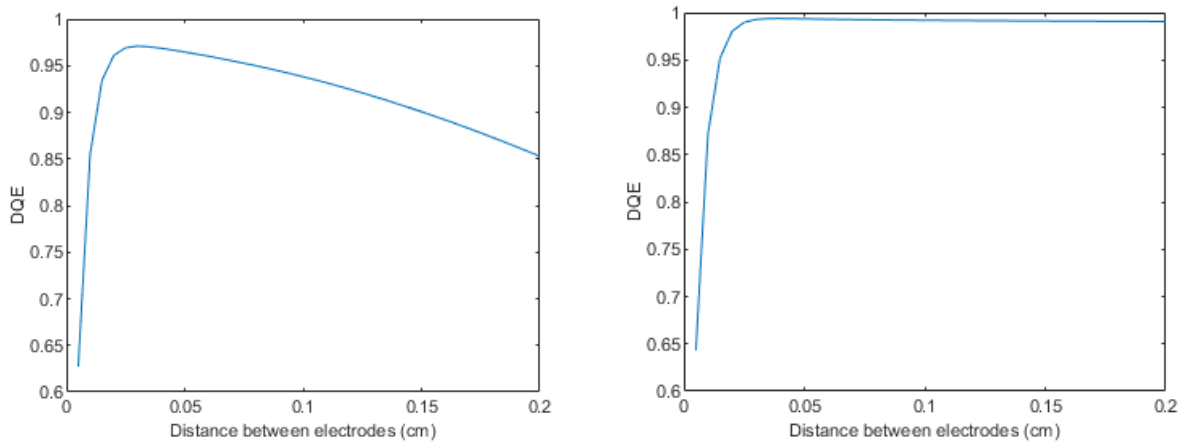

(a) **(b)**

Figure 4.19: Mammography application for folded amorphous Se X-ray detector. Detective quantum efficiency (DQE) as a function of photoconductor thickness d. (a) photon energy E=20keV, hole mobility μ_h=0.12 $cm^2V^{-1}s^{-1}$, electron mobility μ_e=0.003 $cm^2V^{-1}s^{-1}$, hole lifetime τ_h=50 μs, electron lifetime τ_e=200 μs, exposure X= 0.6 mR, Electrical noise Ne=500e, (b) photon energy E=20keV, hole mobility μ_h=0.12 $cm^2V^{-1}s^{-1}$, electron mobility μ_e=0.003 $cm^2V^{-1}s^{-1}$, hole lifetime τ_h=50 μs, electron lifetime τ_e=200 μs, exposure X= 240 mR, Electrical noise Ne=500e.

Figure 4.19 shows the affect of change in electrode distance *d* on DQE for fluoroscopy application in conventional structure. In conventional structure, distance between electrodes is considered as photoconductor thickness. The applied electric field was F=10 V/μm and incident photon energy was E=20keV. The nominal exposure of X=0.6 mR was used in figure 4.19a, and X=240 mR was used for figure 4.19b. The electron hole pair (EHP) creation energy $W_{\pm}$ was

45eV [29]. Electronic noise was 500e. Hole mobility μ_h=0.12 $cm^2V^{-1}s^{-1}$, electron mobility μ_e=0.003 $cm^2V^{-1}s^{-1}$, hole lifetime τ_h=50 µs, and electron lifetime τ_e=200 µs.

In figure 4.19a, DQE reaches the peak value (0.97) for thickness of 0.035cm, then it drops rapidly with increase of distance between charge collecting electrodes. In figure 4.19b, the DQE increases with the photoconductor thickness gradually, and after reaching the peak value of DQE at a certain thickness (0.99 at 0.03cm), DQE starts to drop slowly if thickness is increased further.

When noise=1000e and Photon energy=20keV (Negative bias)

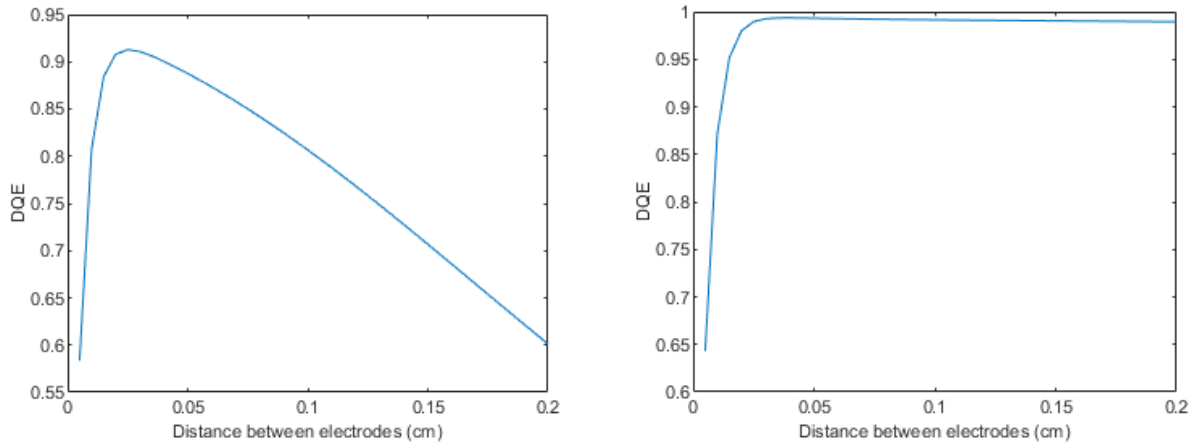

(a) **(b)**

Figure 4.20: Mammography application for folded amorphous Se X-ray detector. Detective quantum efficiency (DQE) as a function of photoconductor thickness d. (a) photon energy E=20keV, hole mobility μ_h=0.12 $cm^2V^{-1}s^{-1}$, electron mobility μ_e=0.003 $cm^2V^{-1}s^{-1}$, hole lifetime τ_h=50 µs, electron lifetime τ_e=200 µs, exposure X= 0.6 mR, Electrical noise Ne=1000e, (b) photon energy E=20keV, hole mobility μ_h=0.12 $cm^2V^{-1}s^{-1}$, electron mobility μ_e=0.003 $cm^2V^{-1}s^{-1}$, hole lifetime τ_h=50 µs, electron lifetime τ_e=200 µs, exposure X= 240 mR, Electrical noise Ne=1000e.

Figure 4.20 shows the affect of change in electrode distance *d* on DQE for fluoroscopy application in conventional structure. In conventional structure, distance between electrodes is considered as photoconductor thickness. The applied electric field was F=10 V/µm and incident photon energy was E=20keV. The nominal exposure of X=0.6 mR was used in figure 4.20a, and

X=240 mR was used for figure 4.20b. The electron hole pair (EHP) creation energy $W_{\pm}$ was 45eV [29]. Electronic noise was 1000e. Hole mobility μ_h=0.12 $cm^2V^{-1}s^{-1}$, electron mobility μ_e=0.003 $cm^2V^{-1}s^{-1}$, hole lifetime τ_h=50 μs, and electron lifetime τ_e=200 μs.

In figure 4.20a, DQE reaches the peak value (0.91) for thickness of 0.03cm, then it drops rapidly with increase of distance between charge collecting electrodes. In figure 4.20b, the DQE increases with the photoconductor thickness gradually, and after reaching the peak value of DQE at a certain thickness (0.99 at 0.03cm), DQE starts to drop slowly if thickness is increased further.

4.3.2: Summary of the graphs for Amorphous Selenium

In table 4.5, we have gathered information about the optimum photoconductor thickness l^* and distance between electrodes d^* in different conditions in folded structure for fluoroscopy application. Hole mobility μ_h=0.12 $cm^2V^{-1}s^{-1}$, electron mobility μ_e=0.003 $cm^2V^{-1}s^{-1}$, hole lifetime τ_h=50 μs, electron lifetime τ_e=200 μs. For different values of exposure, we get different flux. For lower flux, when electronic noise is 1000e, when detector thickness is more than 0.16 cm and distance between electrodes is between 0.025cm and 0.05cm, then we get DQE to be more than 0.3, but if the distance between electrodes is more than 0.05cm, then DQE drops below 0.3. Similarly for higher flux, when electronic noise is 2000e, we get DQE to be more than 0.7 for detector thickness more than 0.18 cm and distance between electrodes is between 0.0025cm and 0.05cm.

Folded Structure, Fluoroscopy						
E=60 keV	l^* (cm)	d^* (cm)	DQE for ψ_{Low}	l^* (cm)	d^* (cm)	DQE for ψ_{High}
Electronic Noise 1000e	>0.18	0.025-0.05	>0.5	>0.17	0.025-0.175	>0.8

Electronic Noise 2000e	>0.15	0.025-0.075	>0.2	>0.18	0.025-0.125	>0.8

Table 4.5: Design guideline for fluoroscopy application for folded amorphous selenium X-ray detector. For photon energy E=60keV, performance of DQE is measured for low (0.1μR) and high exposure (10μR) along with different electronic noise (1000e and 2000e).

In table 4.6, we have gathered information about the optimum photoconductor thickness l^* and distance between electrodes d^* in different conditions in folded structure for mammography application. While using lower flux and electronic noise of 500e, when detector thickness is more than 0.02 cm and distance between electrodes is between 0.025cm and 0.05cm, then we get DQE to be more than 0.8, but if the distance between electrodes is more than 0.05cm, then DQE drops below 0.8. Again, for the same case, if electronic noise is more (1000e), the DQE decreases for the same range of photoconductor thickness and electrode distance (DQE=0.7).

Folded Structure, Mammography						
E=20 keV	l^* (cm)	d^* (cm)	DQE for ψ_{Low}	l^* (cm)	d^* (cm)	DQE for ψ_{High}
Electronic Noise 500e	>0.01	0.025-0.5	>0.8	>0.01	0.025-0.5	>0.8
Electronic Noise 1000e	>0.01	0.025-0.2	>0.8	>0.01	0.025-0.5	>0.8

Table 4.6: Design guideline for mammography application for folded amorphous selenium X-ray detector. For photon energy E=20keV, performance of DQE is measured for low (0.6mR) and high exposure (240mR) along with different electronic noise (500e and 1000e).

In table 4.7, we have gathered information about the optimum distance between electrodes d^* in different conditions in conventional structure for fluoroscopy application for both positive and negative biasing. We can see for photon energy E=60keV, we have figured out ranges for optimum distance between electrodes d^* for specific values of DQE. While using lower flux, electronic flux of 1000, positive biasing, when distance between electrodes is more than 0.08cm,

we get DQE to be more than 0.1, but if the distance between electrodes is less than 0.08cm, then DQE drops below 0.1. Again, for higher flux (higher exposure), electronic flux of 1000e, negative biasing, if distance between electrodes is more than 0.06 cm, we get DQE to be more than 0.07. But if distance between electrodes is more than 0.06cm, than DQE drops below 0.07. Using amorphous selenium, we obtain very low values of DQE compared to poly-$MAPbI_3$ for fluoroscopy application.

Conventional Structure, Fluoroscopy					
E=60 keV		d^* (cm)	DQE for ψ_{Low}	d^* (cm)	DQE for ψ_{High}
Electrical Noise 1000e	Positive bias	>0.17	>0.4	>0.19	>0.8
	Negative bias	>0.12	>0.3	>0.14	>0.7
Electrical Noise 2000e	Positive bias	>0.19	>0.18	>0.19	>0.8
	Negative bias	>0.1	>0.1	>0.16	>0.7

Table 4.7: Design guideline for fluoroscopy application for conventional amorphous selenium X-ray detector. Both positive and negative biasing was observed. For photon energy E=60keV, performance of DQE is measured for low (0.1μR) and high exposure (10μR) along with different electronic noise (1000e and 2000e).

In table 4.8, we have gathered information about the optimum distance between electrodes d^* in different conditions in conventional structure for mammography application for both positive and negative biasing. While using lower flux, electronic flux of 500, positive biasing, when distance between electrodes is more than 0.015cm, we get DQE to be more than 0.8, but if the distance between electrodes is less than 0.015cm, then DQE drops below 0.8. Again, for higher flux (higher exposure), electronic flux of 1000e, negative biasing, if distance between electrodes is more than 0.01 cm, we get DQE to be more than 0.8. But if distance between electrodes is less than 0.01cm, than DQE drops below 0.8. Using amorphous selenium, we obtain almost similar DQE compared to poly-$MAPbI_3$ for mammography application.

Conventional Structure, Mammography					
E=20 keV		d^* (cm)	DQE for ψ_{Low}	d^* (cm)	DQE for ψ_{High}
Electrical Noise 500e	Positive bias	>0.01	>0.8	>0.01	>0.8
	Negative bias	>0.01	>0.8	>0.01	>0.8
Electrical Noise 1000e	Positive bias	>0.01	>0.8	>0.01	>0.8
	Negative bias	0.01-0.09	>0.8	>0.01	>0.8

Table 4.8: Design guideline for mammography application for conventional amorphous selenium X-ray detector. Both positive and negative biasing was observed. For photon energy E=20keV, performance of DQE is measured for low (0.6mR) and high exposure (0.6mR) along with different electronic noise (500e and 1000e).

4.4: Comparison between a-Se and poly-$MAPbI_3$ X-ray Detectors

Both conventional structure and folded structure have been examined for fluoroscopy and mammography for amorphous selenium and poly-$MAPbI_3$. From table 4.1-4.8, it has been found that amorphous selenium and poly-$MAPbI_3$ both provide optimum performance for mammography in conventional structure (From table 4.4 and 4.8). But folded structure of poly-$MAPbI_3$ provides relatively better performance than conventional structure for mammography application using both materials (From table 4.2). For fluoroscopy application, folded structure using poly-$MAPbI_3$ shows relatively better performance than both poly-$MAPbI_3$ conventional structure and *a-Se* structure (folded and conventional) (from table 4.1,4.3,4.5,4.7). Therefore, we can conclude that poly-$MAPbI_3$ provides better DQE performance than *a-Se* for both applications.

Chapter 5: Summary, Conclusion, and Future work

5.1 Summary

The DQE of the folded device structure, which includes incomplete charge collection, was calculated using a cascaded linear system model. For different values of incident photon flux, attempts were made to determine the optimum folding length and thickness of the detector. Random charge carrier trapping was considered, leading to the consideration of variance in charge collection efficiency. In general, it has been observed that when the photoconductor thickness is increased, a rising behavior in the detective quantum efficiency (DQE) is exhibited for folded structure. 3D curves were simulated to observe the change in DQE with variations in the length and thickness of the detector, and the optimum size was determined. Following that, the same thickness of detector was considered for the conventional structure using the respective incident flux. A significant difference in DQE between conventional and folded devices can be clearly observed. Much better performance in terms of detective quantum efficiency (DQE) is exhibited by folded devices compared to the conventional structure. Simultaneously, a comparative study was conducted between amorphous selenium and poly-$MAPbI_3$ X-ray detectors. The work was published with the title "**Comparative Performance Evaluation of Conventional and Folded Detector Structures: Application to Perovskite X-ray Detectors**" in journal "Electronics," by the publisher "MDPI," in Volume 12, Issue 13, page number 2976, on 6th July 2023, where the imaging performance of the conventional and folded detector structure had been studied using poly $MAPbI_3$ for both fluoroscopy and mammography.

5.2 Conclusion

The DQE performance of both folded and conventional detector structures has been analyzed by considering the quantum noise due to random charge carrier trapping in the photoconductor layer in the cascaded linear system model. An analytical expression for the variance of incomplete charge collection in folded structure has also been developed. The optimum values of photoconductor layer thickness l and spacing between electrodes d for maximizing the DQE

under various combinations of exposure, electronic noise and $\mu\tau$ have been determined. The folded structure provides design flexibility for achieving DQE higher than 0.7 by adjusting the distance between electrodes while the maximum possible DQE in conventional structure can be even below 0.3 for certain values of material and detector parameters. The DQE model for folded structure in this paper can also be applied to coplanar detector structure if the electric field profile is considered uniform. At the same time, a comparison has been drawn between poly-$MAPbI_3$ and amorphous selenium, and it has been found that poly-$MAPbI_3$ detector shows significantly better DQE performance than Amorphous Selenium Detector.

5.3 Future work

The photoconductor structures in this thesis were developed for zero spatial frequency. But spatial spreading of signal is an unavoidable fact in imaging system. Taking spatial frequency into account to determine DQE will provide better understanding of the relative increase of noise of the imaging system. Deriving DQE as a function of spatial frequency will help to compare folded and conventional device structure in a broader perspective. Moreover, in the thesis, optimum design parameters of folded and conventional device structure were investigated for fluoroscopy and mammography, but many other medical applications such as tomosynthesis and chest radiology should be brought under evaluation. Furthermore, in this thesis, only the relative comparison between amorphous selenium and poly-$MAPbI_3$ were presented, but different other types of Hybrid Organic-Inorganic Perovskite materials can also be used different medical applications such as tomosynthesis, chest radiology, fluoroscopy, and mammography.

REFERENCES

[1] A. Hessenbruch, “A brief history of X-rays”, ELSEVIER, Volume 26, Issue 4, Pages 137-141, 2002

[2] M. Overdick, C. Bäumer, K. J. Engel, J. Fink, C. Herrmann, H. Krüger, M. Simon, R. Steadman, and G. Zeitler, “Status of Direct Conversion Detectors for Medical Imaging with X-rays”, IEEE Transactions on Nuclear Science, Volume 56, Issue 4, 1800–1809, 2009.

[3] M. Persson, R. Bujila, P. Nowik, H. Andersson, L. Kull, J. Andersson, H. Bornefalk, M. Danielsson, “Upper limits of the photon fluence rate on CT detectors: Case study on a commercial scanner”, Medical Physics, Volume 43, Issue 7, 4398–4411, 2016.

[4] H. T. V. Dam, S. Seifert, R. Vinke, P. Dendooven, H. Löhner, F. J. Beekman and D. R. Schaart, “A practical method for depth of interaction determination in monolithic scintillator PET detectors”, Physics in Medicine and Biology Volume 56, Issue 13, 4135–4145, 2011.

[5] N. Kotwaliwale, K. Singh, A. Kalne, S. N. Jha, N. Seth, A. Kar, “X-ray imaging methods for internal quality evaluation of agricultural produce”, Journal of Food Science and Technology Volume 51, Issue 1, 1–15, 2014

[6] L. De Chiffre, S. Carmignato, J.-P. Kruth, R. Schmitt, A. Weckenmann, “Industrial applications of computed tomography” CIRP Annals, Volume 63, Issue 2, 655–677, 2014

[7] M. Wevers, B. Nicolaï, P. Verboven, R. Swennen, S. Roels, E. Verstrynge, S. Lomov, G. Kerckhofs, B. V. Meerbeek, A. M. Mavridou, L. Bergmans, P. Lambrechts, J. Soete, S. Claes & H. Claes , “Applications of CT for non-destructive testing and materials characterization”, Industrial X-ray Computed Tomography, 267–331, 2018

[8] D.J. Bull1, L. Helfen, I. Sinclair, S.M. Spearing, T. Baumbach, “A comparison of multi-scale 3D X-ray tomographic inspection techniques for assessing carbon fibre composite impact damage”, Composites Science and Technology, Volume 75, 55–61, 2013.

[9] N. Estre, D. Eck, Jean-Luc Pettier, E. Payan, C. Roure, E. Simon, "High-energy X-ray imaging applied to non destructive characterization of large nuclear waste drums", 3rd International Conference on Advancements in Nuclear Instrumentation, Measurement Methods and their Applications (ANIMMA), IEEE Transactions on Nuclear Science, 1-6, 2013.

[10] L. Stobinski, B. Lesiak, A. Malolepszy, M. Mazurkiewicz, B. Mierzwa, J. Zemek, P. Jiricek, I. Bieloshapka, “Graphene oxide and reduced graphene oxide studied by the XRD, TEM and electron spectroscopy methods”, Journal of Electron Spectroscopy and Related Phenomena, Volume 195, 145–154, 2014.

[11] M. Z. Kabir, “Basic principles of solid state x-ray radiation detector operation”, in Handbook of II-VI Semiconductor-Based Sensors and Radiation Detectors: Vol. 3, Sensors Biosensors and Radiation Detectors, ed. by G. Korotcenkov, (Springer Nature, Switzerland AG, 2023), Chapter 1.

[12] L.E. Antonuk, J.M. Boudry, Y. El-Mohri, W. Huang, J.H. Siewerdsen, J. Yorkston, R.A., “Large-area flat-panel amorphous silicon imagers”, Physics of Medical Imaging, Proc. SPIE Proceedings Volume 2708, 499,1996

[13] S. O. Kasap, "X-ray sensitivity of photoconductors: application to stabilized a-Se," Journal of Physics D: Applied Physics, Volume 33, Issue 21, 2853, 2000.

[14] S. Deumel, A. V. Breemen, G. Gelinck, B. Peeters, J. Maas, R. Verbeek, S. Shanmugam, H. Akkerman, E. Meulenkamp, J. E. Huerdler, M. Acharya, M. G. Batlle, O. Almora, A. Guerrero, G. G. Belmonte, W. Heiss, O. Schmidt & S. F. Tedde , “High-sensitivity high-

resolution X-ray imaging with soft-sintered metal halide perovskites", Nature Electronics, Volume 4, 681–688 ,2021

[15] M. Z. Kabir and S. O. Kasap, Photoconductors for Direct Conversion X-ray Image Detectors, in Springer handbook of electronic and photonic materials, 2nd edition ed. by S. O. Kasap and P. Capper (Springer Academic Publishers, October 2017), Chapter 45, 1125-1147.

[16] S. O. Kasap, J. B. Frey, G. Belev, O. Tousignant, H. Mani, J. Greenspan, L. Laperriere,O. Bubon, A. Reznik, G. DeCrescenzo, K. S. Karim, and J. A. Rowlands, "Amorphous and Polycrystalline Photoconductors for Direct Conversion Flat Panel X-ray Image Sensors", Sensors, Volume 11, Issue 5, 5112 ,2011.

[17] S. Yakunin, M. Sytnyk, D. Kriegner, S. Shrestha, M. Richter, G. J. Matt, H. Azimi, C. J. Brabec, J. Stangl, M. V. Kovalenko & W. Heiss , "Detection of X-ray photons by solution-processed lead halide perovskites," Nature Photonics, volume 9, 444–449, 2015.

[18] S. Yakunin, D. N. Dirin, Y. Shynkarenko, V. Morad, I. Cherniukh, O. Nazarenko, D. Kreil, T. Nauser & M. V. Kovalenko, "Detection of gamma photons using solution-grown single crystals of hybrid lead halide perovskites," Nature Photonics, volume 10, Issue 9, 585-589, 2016.

[19] M. Spahn, "X-ray detectors in medical imaging", Nuclear Instruments and Methods in Physics Research, Section A: Accelerators, Spectrometers, Detectors and Associated Equipment, Volume 731, 57–63, 2013

[20] J.A. Rowlands, W. Zhao, "Towards a digital radiology roadmap" ECS Transactions, Volume 54, Issue 1, 293–303, 2013

[21] A.R. Cowen, A.G. Davies, M.U. Sivananthan, “The design and imaging characteristics of dynamic, solid-state, flat-panel X-ray detectors for digital fluoroscopy and fluorography” Clin Radiol , Volume 63, Issue 10, 1073–1085, 2008

[22] D.M. Schlosser, M. Huth, R. Hartmann, A. Abboud, S. Send, T C. Nurdan, M. Shokr, U. Pietsch, L. Strüder, “Direct and indirect signal detection of 122 keV photons with a novel detector combining a pnCCD and a CsI (Tl) scintillator.” Nuclear Instruments and Methods in Physics Research, Section A: Accelerators, Spectrometers, Detectors and Associated Equipment, Volume 805, 55–62, 2016

[23] Kabir, M.Z. “X-ray Photoconductivity and Typical Large Area X-ray Photoconductors.” In Photoconductivity and Photoconductive Materials; Kasap, S.O., Ed. Wiley & Sons: Chichester, UK, 2022; Chapter 15.

[24] S. Kasap, J.B. Frey, G. Belev, O. Tousignant, H. Mani, J. Greenspan, L. Laperriere, O. Bubon, A. Reznik, G. DeCrescenzo, K.S. Karim, J.A. Rowlands, “Amorphous and Polycrystalline Photoconductors for Direct Conversion Flat Panel X-ray Image Sensors.” Sensors, Volume 11, Issue 5, 5112–5157, 2011

[25] S. Yakunin, M. Sytnyk, D. Kriegner, S. Shrestha, M. Richter, G. Matt, H. Azimi, C. Brabec, J. Stangl, M. Kovalenko, W. Heiss, “Detection of X-ray photons by solution-processed lead halide perovskites.” Nature Photonics, Volume 9, 444, 2015

[26] Y.C. Kim, K.H. Kim, D.Y. Son, D.N. Jeong, J.Y. Seo, Y.S. Choi, I.T. Han, S.Y. Lee, N.G. Park, “Printable organometallic perovskite enables large-area, low-dose X-ray imaging.” Nature, Volume 550, 87-91, 2017

[27] M.Z. Kabir, S. Kasap, “Modulation transfer function of photoconductive X-ray image detectors: Effects of charge carrier trapping.” Journal of Physics D: Applied Physics , Volume 36, 2352–2358, 2003

[28] M.Z. Kabir, S. Kasap, “DQE of photoconductive X-ray image detectors: Application to a-Se.” Journal of Physics D: Applied Physics, Volume 35, 2735–2743, 2002

[29] H. Mescher, E. Hamann, U. Lemmer, “Simulation and design of folded perovskite X-ray detectors.” Scientific Reports, Volume 9, 5231, 2019

[30] D.M. Hunter, J.A. Rowlands, “Differences between transient photoconductivity in a-Se sandwich(bulk) and co-conventional(interface) structures.” Journal of Materials Science: Materials in Electronics , Volume 31, 9114–9125, 2020

[31] I. A. Cunningham and R. Shaw, "Signal-to-noise optimization of medical imaging systems," Journal of the Optical Society of America A, volume 16, Issue 3, 621-632, 1999.

[32] J. G. Mainprize, D. C. Hunt, M. J. Yaffe, "Direct conversion detectors: The effect of incomplete charge collection on detective quantum efficiency," medical physics, volume 29, Issue 6, 976-990, 2002.

[33] M. Rabbani, R. Shaw, and R.V. Metter, "Detective quantum efficiency of imaging systems with amplifying and scattering mechanisms," Journal of the Optical Society of America A, volume 4, Issue 5, 895-901, 1987.

[34] S. O. Kasap and M. Z. Kabir, “X-Ray Detectors: Direct Conversion Flat Panel X-Ray Imagers”, Springer Handbook of Semiconductor Devices, ed: M. Rudan et al. (Springer Nature, Switzerland AG, 2022), Chapter 20.

[35] I. Cunningham, Applied linear-systems theory, In Handbook of Medical Imaging; J. Beutel, H.L. Kundel, R.L. Van Metter, Eds. SPIE Press: Washington, DC, USA, 2000, Volume 1, Chapter 2

[36] W. Zhao, W.G. Ji, A. Debrie, J.A. Rowlands, “Imaging performance of amorphous selenium based flat-panel detectors for digital mammography: Characterization of a small area prototype detector.” Medical Physics, Volume 30, Issue 2, 254–263, 2003

[37] M.Z. Kabir, E.V. Emelianova, V.I. Arkhipov, M. Yunus, G. Adriaenssens, S.O. Kasap, “The effects of large signals on charge collection in radiation detectors: Application to amorphous selenium detectors.” Journal of Applied Physics , Volume 99, 124501, 2006

[38] M.Z. Kabir, “Effects of charge carrier trapping on polycrystalline PbO X-ray imaging detectors.” Journal of Applied Physics, Volume 104, 074506, 2008

[39] J.G. Mainprize, D.C. Hunt, M.J. Yaffe, “Direct conversion detectors: The effect of incomplete charge collection on detective quantum efficiency.” Medical Physics, Volume 29, Issue 6, 976–990, 2002

[40] M.Z. Kabir, S. Kasap, “DQE of photoconductive X-ray image detectors: Application to a-Se.” Journal of Physics D: Applied Physics, Volume 35, 2735–2743, 2002

[42] D. Shi, V. Adinolfi, R. Comin , M. Yuan , E. Alarousu , A. Buin , Y. Chen , S. Hoogland , A. Rothenberger , K. Katsiev , Y. Losovyj , X. Zhang , P. A. Dowben , O. F. Mohammed , E. H. Sargent , O. M. Bakr, "Low trap-state density and long carrier diffusion in organolead trihalide perovskite single crystals," Science, Volume 347, Issue 6221, 519-522, 2015.

[43] M. I. Saidaminov, A. L. Abdelhady, B. Murali, E. Alarousu, V.M. Burlakov, W. Peng , I. Dursun , L. Wang , Y. He, G. Maculan, A. Goriely, T. Wu, O. F. Mohammed, O. M. Bakr, "High-quality bulk hybrid perovskite single crystals within minutes by inverse temperature crystallization," Nature Communications, Volume 6, 7586, 2015.

[44] G. Giorgi and K. Yamashita, "Organic–inorganic halide perovskites: an ambipolar class of materials with enhanced photovoltaic performances," Journal of Materials Chemistry A, Volume 3, Issue 17, 8981–8991, 2015.

[45] J. M. Ball and A. Petrozza, “Defects in perovskite-halides and their effects in solar cells”, Nat Energy, Volume 1, 16149, 2016

[46] J. Rowlands and J. Yorkston, Flat panel detectors for digital radiography, in ‘Handbook of Medical Imaging: vol. 1’ by J. Beutel, H.L. Kundel, and R.L. Van Metter, (Eds.), (SPIE Press, Washington, 2000), ch. 4.